Prefrontal dopamine activity is critical for rapid threat avoidance learning

Zachary Zeidler[1], Marta Fernandez Gomez[2], Tanya A. Gupta[2], Meelan Shari, Scott A. Wilke[2*], and Laura A. DeNardo[1,3**]

[1]Department of Physiology; David Geffen School of Medicine, University of California, Los Angeles, California.

[2]Department of Psychiatry, Semel Institute for Neuroscience and Human Behavior, David Geffen School of Medicine, University of California, Los Angeles, California.

[3]Lead contact

[*]Correspondence: ldenardo@ucla.edu; swilke@mednet.ucla.edu

Short title: prefrontal dopamine promotes avoidance learning

Pages: 33

Figures: 7

Abstract: 177 words

Introduction: 579 words

Discussion: 1204 words

Conflict of interest: The authors declare no competing financial interests.

Keywords: prefrontal cortex, dopamine, avoidance learning, platform-mediated avoidance, GRABDA.

Abstract

The medial prefrontal cortex (mPFC) is required for learning associations that determine whether animals approach or avoid potential threats in the environment. Dopaminergic (DA) projections from the ventral tegmental area (VTA) to the mPFC carry information, particularly about aversive outcomes, that may inform prefrontal computations. But the role of prefrontal DA in learning based on aversive outcomes remains poorly understood. Here, we used platform mediated avoidance (PMA) to study the role of mPFC DA in threat avoidance learning in mice. We show that activity in VTA-mPFC dopaminergic terminals is required for avoidance learning, but not for escape, conditioned fear, or to recall a previously learned avoidance strategy. mPFC DA is most dynamic in the early stages of learning, and encodes aversive outcomes, their omissions, and threat-induced behaviors. Computational models of PMA behavior and DA activity revealed that mPFC DA influences learning rates and encodes the predictive relationships between cues and adaptive behaviors. Taken together, these data indicate that mPFC DA is necessary to rapidly learn behaviors required to avoid signaled threats, but not for learning cue-threat associations.

Introduction

To thrive in a complex environment, animals must seek beneficial outcomes while avoiding threats. Natural environments are highly dynamic, requiring individuals to continuously update predictive relationships between stimuli, actions, and outcomes. Threat learning must occur rapidly and reliably to avoid injury or death. But excessively avoiding threats can also limit opportunities to engage in beneficial pursuits. Thus, appropriately balancing approach and avoidance in a threatening context is critical. Moreover, disturbances in this balance can lead to maladaptive behaviors characteristic of psychiatric disorders. Thus, it is critical to understand the neurobiological mechanisms mediating rapid threat avoidance learning.

The medial prefrontal cortex (mPFC) is essential for integrating learned information about the environment to guide actions, in particular when resolving approach-avoidance conflicts and

encoding contextual associations with threat and safety[1–7]. Activity in mPFC is likewise critical for both learning to avoid threats and for driving avoidance behavior, especially in situations that involve conflicting motivational drives[8–16]. While much progress has been made in understanding the mPFC mechanisms that drive avoidance behavior, less is known about the prefrontal mechanisms underlying the process of learning these avoidance learning.

Dopamine (DA) is a potent modulator of mPFC function yet is poorly understood in comparison with the mesolimbic DA system[17]. Prefrontal DA has been difficult to study because of the lower density of dopaminergic fibers as well as the lack of tools to monitor DA with high temporal resolution in isolation from other catecholamines[18]. DA axons targeting mPFC arise from the ventral tegmental area (VTA)[19–22]. VTA-mPFC DA neurons do not collateralize and represent a subpopulation with distinct molecular, cellular, and functional properties[23–29]. In contrast to the reward-related functions of mesolimbic DA projections, VTA-mPFC projecting DA neurons and their terminals are preferentially engaged by aversive stimuli[17,20,29–34]. DA is known to play a critical role in aversive learning but has mostly been studied without regional specificity and/or in the context of conditioned fear[35–38]. Some studies suggest that DA plays a key role in threat avoidance, but most used midbrain lesions, global pharmacological inhibition of DA signaling, or microdialysis[39–42]. These approaches lack the spatiotemporal precision required to associate mPFC DA transients with distinct epochs of learning or cannot provide causal information, leaving substantial gaps in our understanding of the role of mPFC DA in learning active strategies to avoid threats.

In this study, we utilized platform mediated avoidance (PMA)[14,15] to investigate the hypothesis that the activity of VTA-mPFC dopaminergic projections is critical for learning to avoid aversive outcomes. We further hypothesized that this relationship is distinct from stimulus-outcome associative learning that lacks a learned behavioral response. To test this, we combined terminal-specific optogenetic inhibition of VTA-mPFC DA projections, fiber photometry recordings of mPFC DA release, and computational modeling of mPFC DA dynamics and behavior. Our

findings reveal a critical role for mPFC DA in signaled avoidance learning but not in retrieval of learned avoidance strategies or cue-shock associative learning. To understand the specific patterns of mPFC DA activity underlying threat avoidance learning, we also recorded mPFC DA activity during cued fear conditioning, where avoidance is not possible, and during a yoked control assay, in which shocks are unavoidable and the cue-shock relationship is unpredictable. Using a temporal difference model of mPFC DA activity, we identified unique mPFC DA dynamics specific to avoidance learning, contrasting with cued and yoked fear conditioning assays. Together, our results demonstrate that VTA-mPFC DA circuit activity is necessary to link predictive cues to adaptive behaviors that preempt an aversive outcome.

Results

Mice learn tone-shock relationships and avoidance behaviors during PMA

To investigate the role of mPFC DA projections in avoidance learning, we trained mice using a platform-mediated avoidance (PMA) assay. In this assay, mice learn that a tone predicts a foot shock, and then that they can navigate to a safety platform to avoid this shock. A reward port is located on the opposite side of the chamber such that mice must choose between safety and obtaining reward. Mice were first habituated to the chamber and reward port, followed by three days of PMA training (Figure 1A). Each training day consisted of nine pseudorandomly timed 30-second tones that co-terminated with a 2-second mild foot shock (Figure 1B). Mice were free to move throughout the arena, obtain rewards, or access the safety platform. Overhead video recordings were collected, and supervised deep learning was used to track eight anatomical points on their body (Figure 1C).

Successful avoidance trials were defined as those in which mice moved to the safety platform before the shock onset and remained there until the shock was over. Mice demonstrated a steady increase in successful threat avoidance across the training days (Figure 1D). Correspondingly, mice spent a progressively greater proportion of time on the platform during

tone periods as they learned to preemptively avoid the cued shocks (Figure 1E). Freezing behavior remained consistent and did not change significantly across days (Figure 1F). Thus, mice successfully learned the tone-shock relationship and avoidance behavior required to improve their PMA performance across days.

VTA-mPFC DA terminal activity is required for avoidance learning but not for associating a cue with an aversive outcome

To investigate whether DA inputs to mPFC are required for avoidance learning, we optogenetically inhibited VTA-mPFC DA terminals during tone-shock presentations across three days of platform-mediated avoidance (PMA) training. First, we injected an adeno-associated virus (AAV) encoding the Cre-dependent inhibitory opsin Jaws or a control fluorophore (GFP) into the VTA of TH-Cre mice. In these mice, Cre recombinase is expressed under the control of the tyrosine hydroxylase (TH) promoter, restricting Jaws expression to DAergic neurons. Bilateral optic fibers were then implanted above the mPFC to allow optogenetic inhibition of VTA-mPFC DA axon terminals (Figure 2A). Fluorescence imaging revealed GFP-labeled neurons in the VTA and GFP-labeled axons in the mPFC, confirming successful targeting of the circuit (Figure 2B). During training, we inhibited VTA-mPFC DA terminals using constant 635 nm laser light delivered via the implanted fibers during each tone, including the shock period (Figure 2C).

We assessed whether inhibiting VTA-mPFC DA activity affected signaled avoidance behavior and conditioned freezing (which reflects the strength of the tone-shock association) across learning. Jaws-expressing mice had significantly fewer successful avoidance trials compared to GFP controls, particularly on the first day and early in the second day of training (Figure 2D,E). Instead, Jaws mice exhibited a higher proportion of escape trials, where they leapt to the platform after being shocked, with the largest differences evident early in learning (Figure 2D,F). Importantly, VTA-mPFC DA inhibition did not affect freezing behavior to the tone (Figure

2G), nor did it induce real-time place preference or aversion (Figure S1), indicating that activity in this pathway is not inherently rewarding or aversive.

Although mice with VTA-mPFC DA projections inhibited eventually learned the PMA task, we hypothesized that there might be qualitative differences in their avoidance behavior compared to control mice. To test this, we analyzed interactions with the safety platform and reward port during tone presentations, when threat levels are high and avoidance behavior is adaptive, and during the inter-trial intervals (ITI), when threat levels are low and avoidance behavior is maladaptive. During tone periods, Jaws mice displayed shorter average platform bouts, especially on the second day of training (Figure 2H). In contrast, during the inter-trial interval (ITI), Jaws and GFP controls had similarly low platform bout durations (Figure 2I). Both groups showed minimal reward-seeking behavior during the tone (Figure 2J). Yet during the ITI, Jaws mice interacted with the reward port more than controls (Figure 2K), suggesting that inhibiting VTA-mPFC DA terminals did not generally lead to reduced motivation to seek rewards. These findings indicate that VTA-mPFC DA projections are essential for platform mediated avoidance learning, particularly during the early stages, but are not required for tone-shock learning or to successfully escape shocks by leaping to safety.

Prefrontal DA terminals are required for avoidance learning without motivational conflict, but not retrieval of a previously learned avoidance strategy

To better understand the role of VTA-mPFC DA projections in learning and enacting adaptive avoidance strategies, we conducted additional optogenetic experiments in separate groups of mice. First, we tested whether VTA-mPFC DA activity was necessary for learning in a 1-day version of our PMA task that lacked an explicit approach-avoidance conflict (Figure S2A,B). During training, Jaws-expressing mice exhibited fewer successful avoidance trials and more shock-triggered escapes, but no change in tone-elicited freezing (Figure S2C). During a retrieval test the following day (without shocks or optogenetic inhibition), Jaws mice exhibited less time on

the platform with no difference in freezing in response to the tone (Figure S2D). These results are consistent with a selective role for VTA-mPFC DA terminals for linking predictive cues with behaviors that preempt aversive outcomes, even in the absence of motivational conflict.

We next investigated whether inhibiting VTA-mPFC DA terminals were specifically required for avoidance learning, or if they were also required for retrieval of a previously learned avoidance strategy. To test this, we trained a separate cohort of mice in our PMA task, then interleaved trials with or without optogenetic inhibition during retrieval the next day (Figure S2E). Inhibiting VTA-mPFC DA terminals had no effect on either time on platform or freezing to tones during retrieval (Figure S2F,G). Thus, VTA-mPFC DA terminal activity is specifically required to link predictive cues with avoidance behaviors, but not for retrieving a previously learned avoidance strategy.

Inhibiting prefrontal DA terminal activity alters PMA learning rates

To further dissect the role of VTA-mPFC DA terminal activity in avoidance learning, we applied a Rescorla-Wagner learning model[43,44] to our optogenetic behavioral data (Figure 2). This model assumes that the value of the safety platform is updated based on learning rates from shock trials (α). This model successfully captured the learning trajectories of both laser-only control mice (GFP-expressing) and those with inhibited VTA-mPFC DA terminals (Jaws-expressing) (Figure 3B-F), but we observed differences in the learning rates of the GFP and Jaws groups. In GFP- but not Jaws-expressing mice, α tended to decrease across days, suggesting that optogenetic inhibition of VTA-mPFC DA terminals causes a failure to form stable representations of the platform value.

We also considered a different model in which the learning rate was informed by both success ($\alpha_{success}$) and failure ($\alpha_{failure}$) trials. By incorporating value updates driven by both shocks and shock omissions, the model reveals the relative contribution of different trial outcomes to avoidance learning. In control mice, $\alpha_{failure}$ was highest on day 1, indicating that aversive outcomes

primarily drove behavioral adjustments during early learning (Figure S3). But by the second day of training, $\alpha_{success}$ became dominant, suggesting that successful avoidance outcomes guided the majority of behavioral changes during later learning stages (Figure S3). In contrast, Jaws-expressing mice did not exhibit this transition from high $\alpha_{failure}$ to high $\alpha_{success}$. Instead, aversive outcomes continued to drive behavioral changes throughout training (Figure S3). These results suggest that VTA-mPFC DA terminal activity is critical for how aversive outcomes shape future behavior.

Prefrontal DA is most dynamic early in PMA learning and reflects trial outcomes, avoidance behaviors, and threatening locations.

Our optogenetic and modeling data suggested that VTA-mPFC DA terminal activity was most important in the early stages of avoidance learning. However, it was unclear how VTA-mPFC DA terminal activity relates to DA levels in mPFC. To examine this, we expressed the fluorescent DA sensor $GRAB_{DA2m}$[45] (GRABDA) in mPFC and recorded its fluorescence using fiber photometry during PMA training (Figure 4A). Consistent with the critical role of VTA-mPFC DA terminal activity early in learning, we observed the largest mPFC DA dynamics on Day 1 of PMA training (Figure 4B).

To understand how mPFC DA encodes trial outcomes, we examined GRABDA signals during shocks and shock omissions during PMA. Unsuccessful trials that resulted in shocks evoked large initial DA responses that diminished with repeated exposure to the aversive outcome (Figure 4C). Conversely, successful avoidance trials elicited negative DA responses that also diminished with repeated avoids (Figure 4D). Unlike these outcome-specific signals, tone onset responses were smaller and did not consistently vary in magnitude across learning (Figure 4E). GRABDA signals were unrelated to overall movement velocity (Figure 4F), indicating that the observed dynamics did not simply reflect motor activity. Additional controls confirmed that

GRABDA fluorescence reflected DA dynamics rather than movement artifacts: fiber photometry recordings in GFP-expressing animals showed no shock or avoidance responses (Figure S4), and administration of the D2 receptor antagonist eticlopride diminished shock-evoked GRABDA responses (Figure S5).

We observed only small increases in mPFC DA following tone onset, but all animals had fluctuations in mPFC DA throughout the 30-second tone, suggesting some of the activity may relate to specific behaviors. We therefore investigated whether mPFC DA encoded avoidance and freezing behaviors. mPFC DA ramped up during platform entries and returned to baseline upon reaching safety (Figure 4G). Similarly, DA signals increased during platform exits onto the shock grid and remained elevated (Figure 4H). We observed a nonsignificant trend for DA signals to increase before freezing onset (Figure 4I) and decrease before freezing offset (Figure 4J). Together, our findings indicate that mPFC DA encodes trial outcomes, threat-induced behaviors, and threatening locations. Moreover, mPFC DA dynamics are strongest during the early stages of learning.

Removing shock avoidability from PMA alters mPFC DA encoding of trial outcomes and cues.

We found that mPFC DA is dynamically increased in response to an aversive outcome, but is modulated in the opposing direction when mice successfully avoid it, and that learning modulates the amplitude of these signals. This led us to ask whether it was the ability to avoid the shock on a platform or the particular pattern of shocked and non-shocked outcomes that drove these learning-related changes in mPFC DA. To investigate this, we removed the safety platform from the arena, eliminating the ability to intentionally avoid shocks, and then for each mouse in this cohort, we yoked the trials associated with shocks to mice in the PMA group. Thus, both PMA and yoked groups experienced identical patterns of shocked and non-shocked trials. So, in PMA,

shock omissions were associated with platform entries whereas in the yoked controls, there was no discernable relationship between actions and shock omissions. We then used GRABDA to record DA dynamics during this yoked paradigm (Figure 5A,B).

Mice exposed to yoked conditioning exhibited increased freezing to the tone on Day 1 which plateaued on Days 2 and 3 (Figure 5C). We observed DA responses to shocks and tone onsets (Figure 5D) but found that prefrontal DA dynamics were distinct from those seen in PMA. Unlike in PMA, DA response to shocks remained elevated across the session (Figure 5E). Moreover, we did not observe a decrease in mPFC DA during the early shock omissions, but instead saw low DA signals trending towards an increase across the session (Figure 5F). Furthermore, in contrast to PMA, DA levels during the tone onset increased significantly over time (Figure 5G). These findings indicate that the shock omission by nature of platform avoidance, not the pattern of cue-shock pairings, drove the pattern of mPFC DA dynamics we observed. They also suggest that mPFC DA levels are sensitive to both the predictability and to the avoidability of shocks.

Prefrontal DA is not required for cued fear conditioning

While our yoked task design maintained the tone-outcome sequence of PMA, it also introduced uncertainty to the tone-shock relationship. In PMA, the tone-shock relationship is predictable yet avoidable. To examine mPFC DA dynamics when mice learn about shocks that are predictable but unavoidable, we contrasted our previous results with a standard cued fear conditioning assay. We recorded DA dynamics during one day of fear conditioning, in which every tone terminates with an unavoidable shock, and during fear memory retrieval, in which conditioned tones are presented without shocks (Figure 6A,B). Prefrontal DA dynamics during both fear conditioning and retrieval were distinct from those observed in PMA and yoked conditioning (Figure 6C,D). During training, we observed a large increase in mPFC DA during the first shock that steadily declined in amplitude with subsequent shocks (Figure 6E). On the retrieval day, there was a large

increase in DA when the shock was first unexpectedly omitted but that response rapidly diminished with repeated tone presentations (Figure 6F). Tone onset responses during training showed no consistent change (Figure 6G), but during retrieval, they significantly decreased across repeated tone presentations (Figure 6H).

Given that VTA-mPFC DA terminal inhibition only affected avoidance learning and not conditioned freezing in PMA, we hypothesized that VTA-mPFC DA terminals are not required for tone-shock learning. To test this, we suppressed VTA-mPFC DA terminal activity during fear conditioning (Figure 6I). On the training day, both Jaws-expressing and GFP control mice showed increased freezing to the tone, with no differences between groups (Figure 6K). Similarly, on the retrieval day, when tones were presented without shocks or optogenetic inhibition, freezing levels during tone presentations were unaffected (Figure 6L). These results indicate that mPFC DA activity is not essential for learning tone-shock associations, regardless of the availability of an avoidance contingency, but reflects important aspects of cue-outcome learning (e.g. unexpected shocks, expected shocks, and unexpected shock omissions).

Temporal difference model captures assay-specific dynamics governing mPFC DA

To investigate how mPFC DA dynamics support learning across PMA, yoked conditioning, and cued fear conditioning, we applied a temporal difference (TD) learning model to capture DA activity. We hypothesized that similar computational principles might underlie mPFC DA signals during associative aversive learning in general, but that assay-specific features (e.g. predictability of tone-shock relationships and avoidability of shock outcomes) would modulate the temporal dynamics of mPFC DA signals. To examine this, we augmented a standard TD model with an uncertainty parameter (β) as a temporal scaling factor. This parameter allows for flexible temporal dynamics in the modeled DA signal, which may vary with assay-specific demands (Figure 7A). Since our Rescorla-Wagner model of behavior revealed that mPFC DA

activity affects learning based on shocks vs. omissions (Figure S6), we separated trials depending on whether mice experienced a shock or not, and assessed model parameters for each trial case.

The model performed similarly well at predicting mPFC DA activity across PMA, yoked conditioning, and cued fear conditioning (Figure 7B). However, the parameter values required to accurately predict mPFC DA differed significantly across the three assays. In particular, the *uncertainty* factor (β) and *discounting* factor (γ) during shock trials were significantly different (Figure 7C,D). In PMA, β initially increased and then decreased in late learning, while it remained relatively stable in yoked conditioning and sharply decreased across learning in cued fear conditioning (Figure 7C). In contrast, γ initially decreased and then increased in late learning on shocked trials in PMA, while both yoked and cued fear conditioning exhibited an increase in γ that remained stable (Figure 7D). While there were interesting trends across learning in the non-shocked trials, these were not significantly different across assays. Trends in *b* (representing the base level of DA) and α (learning rate) were apparent across learning in both shocked and non-shocked trials, but were also not significantly different between assays (Figure 7E,F). Altogether, these findings suggest that the distinct learning demands of each task – such as the potential to preemptively avoid – shape when and how specific computational principles are implemented, especially during aversive outcomes.

Discussion

We demonstrate a critical role for mPFC DA terminal activity in signaled threat avoidance learning and show that mPFC DA itself is linked to specific aspects of the learning process. During threat avoidance learning, DA encodes predictive cues, aversive outcomes and their omission, and threat-related behaviors. Trial-by-trial mPFC DA, measured during avoidance learning, exhibited distinct dynamics in response to conditioned cues, foot shocks and shock omissions compared with assays lacking an avoidance contingency. These data reveal that prefrontal DA dynamics

306 are sensitive to both the predictability and avoidability of aversive outcomes. Consistent with these
307 observations, inhibiting VTA-mPFC DA terminal activity significantly slowed avoidance learning
308 in PMA. In contrast, VTA-mPFC DA terminal activity was not required to link a predictive cue to a
309 passive freezing response, regardless of the avoidability of the shock. This causal dissociation
310 underscores a specialized role for prefrontal DA inputs in rapidly linking predictive cues with
311 behaviors required to actively avoid aversive outcomes.

312 The DA system has a well-established role in associative learning, but most studies have
313 examined the role of striatal dopamine in reward-based learning. However, more recent studies
314 have begun to elucidate a key role for DA in aversive learning as well[22,32,46]. In particular, VTA DA
315 neurons projecting to mPFC appear to be specialized for aversive processing[28–30,47,48] and
316 aversive stimuli drive increases in mPFC DA release[32,46,49,50]. Optogenetic stimulation of prefrontal
317 DA terminals biases behavior towards aversive rather than appetitive behavioral responses[31].
318 Prefrontal DA is also increased during fear conditioning, and prefrontal DA is implicated in the
319 acquisition of contextual fear, and in the expression but not in the acquisition of a tone-shock
320 association[36–38,51–55]. These findings are in agreement with ours and highlight a key role for mPFC
321 DA in learned fear, and suggest prefrontal DA plays different roles depending on the behavioral
322 demands of aversive tasks.

323 Previous studies have also suggested a role for mPFC DA in threat avoidance. However,
324 most of these studies focused on already fully-learned avoidance, not its acquisition. Thus the
325 dopaminergic circuit mechanisms supporting rapid avoidance learning have remained poorly
326 understood. Moreover, previous studies have primarily used lesions and systemic pharmacology
327 as causal manipulations, or microdialysis to measure DA responses. These approaches lack the
328 spatiotemporal precision required to associate DA activity with distinct epochs of learning. Studies
329 that used optogenetics to examine the role of VTA-mPFC DA circuit activity in real-time or
330 conditioned place avoidance yielded mixed results, some finding that stimulation is sufficient to
331 enhance anxiety-like behaviors and promote conditioned place preference[47], and others finding

no effect[17,60]. So, while these studies indicated that mPFC DA activity may have a key role in threat avoidance, the role of mPFC DA in learning to preemptively avoid threats remains poorly understood.

We addressed this important question by using optogenetics and fiber photometry to precisely manipulate and record mPFC DA activity during PMA. Consistent with previous microdialysis studies that examined prefrontal dopamine in a shuttle-box assay[42], we found that during both PMA and fear conditioning, mPFC DA levels were highest early in learning. While aversive foot shocks initially elicited large positive DA responses across all assays, in line with previous studies[20,30,46,61], learning-related changes in the amplitude of these signals depended on the behavioral context. Predictable shocks (during PMA and FC) elicited responses that diminished across learning, while unpredictable shocks (during the yoked assay) did not. Relatively, the increases in mPFC DA seen during conditioned tones and threat-induced behaviors were small. During shock omissions, mPFC DA initially decreased in PMA but increased during fear memory retrieval before diminishing. This builds on previous work showing that VTA-mPFC projections regulate fear extinction learning[62–66], revealing the rapid adaptation of prefrontal DA responses during extinction trials. Together, these findings suggest that, rather than driving specific behaviors, large fluctuations in mPFC DA may enable learning-related circuit plasticity that is required for individuals to flexibly link predictive cues with adaptive actions required for avoidance.

In line with this, we show that inhibition of VTA-mPFC DA slows avoidance learning in PMA. Indeed, our Rescorla-Wagner model of PMA behavior suggested that inhibiting VTA-mPFC DA impeded the animals' ability to use information about aversive outcomes to update the value of a safe location. Our temporal difference model of mPFC DA activity revealed that in the PMA condition, *uncertainty* and *future discounting* parameters decreased across learning in shock trials. In contrast, yoked and fear conditioned groups showed less change in *future discounting*

during shock trials, reflecting more stability in the weight of future predictions. These parameters suggest that, as animals learn to avoid signaled threats, dopamine increasingly encodes the predictive relationships between cues and behavioral strategies required to avoid aversive outcomes. In contrast to PMA, VTA-mPFC DA activity is not required for learning cue-shock associations. This behavioral distinction may reflect the general function of mPFC, which is not required for tone-shock learning[67], but rather for learning to appropriately coordinate actions to support goals[68–70]. Overall, our findings align with evidence that the mPFC plays a critical role in context-dependent learning and application of rule-based behaviors[64–67], and suggest mPFC DA to be a key mechanism guiding adaptive responses to contextual contingencies.

Through associative learning, mPFC circuits integrate information about environmental cues and internal goals to promote adaptive action selection. Activation of DA receptors in the mPFC modulates neuronal excitability and long-term synaptic plasticity[75–77], which may enable rapid learning of avoidance behaviors. DA influences activity primarily via D1 and D2 receptor classes, which are expressed in largely non-overlapping prefrontal cell types[78–81]. mPFC D1 receptor-expressing neurons have strong projections to cortical and thalamic targets[82] and recent evidence shows that DA enhances the signal-to-noise ratio in classes of mPFC projection neurons that encode aversive stimuli[31]. Given that classes of mPFC projection neurons play unique roles in threat avoidance learning[13,83], mPFC DA likely shapes cortical network activity to enhance activity in particular neuronal classes during avoidance learning.

Our study causally manipulated the activity of VTA-mPFC DA terminals during behavioral assays. Since we performed these experiments in TH-Cre mice, the effects we observed were likely related to DA activity. However, recent studies showed that a subset of TH+ VTA cells also co-express the vesicular glutamate transporter VGLUT2[84] and mesocortical DA neurons may co-release glutamate[76]. A more complete understanding of how these projections drive plasticity and learning will require investigation of whether observed effects arise specifically from DA vs. other

co-transmitters, temporally precise manipulations during isolated events (e.g. only during shocks), and examination of how activity arising from VTA-mPFC terminals influences mPFC microcircuit activity.

Altogether, our findings reveal that mPFC DA plays a distinct and essential role in avoidance learning by dynamically encoding trial outcomes and using them to update behavioral strategies. This specialization enables animals to rapidly adapt their behavior in complex environments, linking predictive cues to goal-directed avoidance strategies. By dissociating the roles of mPFC DA in avoidance learning and fear conditioning, this study advances our understanding of the contribution of prefrontal DA to adaptive behavior. These findings also have significant implications for understanding disorders characterized by maladaptive avoidance, such as anxiety, PTSD, and OCD[86,87]. Disruptions in mesocortical dopamine signaling could impair the ability to link predictive cues with adaptive avoidance behaviors, contributing to pathological avoidance or excessive fear responses.

Materials and Methods

All experiments were conducted in accordance with procedures established by the administrative panels on laboratory animal care at the University of California, Los Angeles.

Animals Adult male and female C57Bl6/J mice (JAX stock #000664) or tyrosine hydroxylase Cre (TH-Cre; line Fl12; www.gensat.org) mice were group housed (two to five per cage) and kept on a 12/12 h light/dark cycle (lights on 7AM to 7PM). Mice were sexed by examination of external genitalia at weaning. Animals received *ad libitum* food and water.

Surgery Mice were induced in 5% isoflurane in oxygen until loss of righting reflex and transferred to a stereotaxic apparatus where they were maintained under 2% isoflurane in oxygen. Mice were warmed with a circulating water heating pad throughout surgery and ophthalmic ointment was applied to the eyes. The head was shaved and prepped with three scrubs of alternating betadine and then 70% ethanol. Following a small skin incision, a dental drill was used to drill through the skull above the injection targets. A syringe pump (Kopf, 693A) with a Hamilton syringe was used for injections. Injections were delivered at a rate of 100 nl/min and the syringe was left in the brain for 10 min following injection. For optogenetics experiments, animals were injected with 500nL of AAV5-CAG-FLEX- JAWS-KGC-GFP-ER2 (Addgene #84445) or AAV5-CAG-FLEX-EGFP-WPRE (Addgene #51502) at a titer of $5x10^{12}$ vg/mL bilaterally into the VTA (AP: -2.9 & -2.6 mm, ML: +/- 0.45 mm, DV: -4.5 mm from bregma). Bilateral optic fibers (200 µm core, Newdoon) were implanted over the prelimbic (PL) area of the mPFC (AP: +1.8, ML: +/- 0.35, DV: -1.8 mm from bregma). For fiber photometry experiments, AAV5-hSyn-GRAB_DA2m ($1x10^{13}$ vg/mL) was injected unilaterally into PL (AP: +1.8, ML: -0.35, DV: -2 mm from bregma) with an optic fiber (400 µm core, Doric) implanted 200 µm above it. For pain management mice received 5 mg/kg carprofen diluted in 0.9% saline subcutaneously. Mice received one injection during surgery and

daily injections for 2 d following surgery. For optogenetic experiments, we waited at least four weeks after surgery before experimentation.

Behavior

Platform mediated avoidance

Three days prior to starting PMA, citric acid (2% w/v) was added to animals' drinking water. This self-initiates a reduction in water consumption and increases performance on liquid reward tasks similar to forced water restriction[88]. Animals were then placed into a 20x22cm arena with metal rod flooring (Lafeyette Instruments) and a plexiglass platform covering one-quarter of the floor space. Opposite the platform was a reward port and reward pump (Campden Instruments). The reward port featured an infrared beam that triggered 25 µL of 10% sweetened condensed milk (Nestle) reward on a variable interval schedule (mean interval: 30 seconds). Once a day for two days, animals were placed in the arena and allowed to freely explore and consume reward for 45 minutes. The following day, PMA training began. For three days, animals were placed into the arena with a 180 second baseline period followed by delivery of a 30 second, 75 dB, 4kHz tone that co-terminated with a 2 second, 0.15 mA shock delivered to the floor (Lafeyette Instruments). Eight subsequent tone-shock pairings were delivered at randomly chosen intervals between 80 and 160 seconds. Training on PMA continued for two more days for a total of three days. Data presented in tone blocks are the average performance over three tones.

Fear conditioning and yoked outcomes

For cued fear conditioning, animals were placed in the same arena as PMA without the platform or reward port. On training day, animals received three tones (4 kHz, 10s duration) to assess baseline freezing followed by twelve tones that were paired with a coterminal footshock identical to PMA. The following day (recall), animals were exposed to six tones (4 kHz, 30s duration) unpaired with shock.Data are presented as individual tones. For yoked fear conditioning, the

same arena as cued fear conditioning was used. Trial outcomes for individual subjects were matched to a PMA subject. On each of three days of training, subjects experienced nine tones (4 kHz, 30s duration) and based on the outcome of the matched PMA subject (avoid or shock), the shock was either omitted (for avoid outcome) or delivered (for shock outcome). Data presented in tone blocks are the average performance over three tones.

Optogenetics

JAWS activation was achieved via continuous red light (635 nm, 10 mW, Shanghai Laser and Optics Century) delivered through the entirety of the tone-shock periods. For PMA, laser illumination was concurrent with all the tones. For fear conditioning, this occurred on the first day (training).

Real-time place preference

After PMA, a subset of animals were placed in a real-time place preference (RTPP) assay. Animals were placed in a 68 x 23 cm chamber for 20 minutes. During the first ten minutes, the animals freely explored the arena to establish a baseline side preference. During the subsequent ten minutes, a closed loop video monitoring system (Bioviewer) tracked the location of the animal and triggered a 635 nm laser when the animal entered the “laser” side of the arena. The ratio of time spent in the “non-laser” side of the arena to the “laser” side of the arena was calculated for both baseline (laser off) and test (laser on) periods.

Fiber photometry

Recordings were performed using a commercial fiber photometry system (RZ10x, Tucker Davis Technologies) with two excitation wavelengths, 465 and 405 nm, modulated at 211 and 566 Hz respectively. Light was filtered and combined by a fluorescent mini cube (Doric Lenses). Emission was collected through the mini cube and focused onto a femtowatt photoreceiver (Newport, Model

2151). Samples were collected at 1017 Hz and demodulated by the RZ10x processor. Time stamps to synchronize experimental events and recordings were sent via TTLs to the RZ10x system via Arduino, controlled by custom MATLAB (MathWorks) code. For trial outcome specific analyses, trials were binned into groups of three as done earlier, using three subsequent trials of the same outcome to account for the stochastic nature of trial outcomes in PMA and yoked fear conditioning experiments.

Histology Animals were deeply anesthetized with isoflurane and transcardially perfused with phosphate buffered saline (PBS), followed by 4% paraformaldehyde (PFA). Brains were removed and post-fixed overnight in 4% PFA before being moved to PBS. Brains were then sectioned via vibratome at 60 microns. To detect VTA axons expressing JAWS-GFP in the mPFC, anti-GFP immunohistochemistry was performed. Sections were incubated with chicken anti-GFP polyclonal antibody (1:2000, Aves Labs) overnight at 4℃. Sections were next rinsed and incubated with donkey anti-chicken AlexaFluor 488 conjugate (1:500; Jackson ImmunoResearch) at room temperature for 2 hr. Sections were washed before being mounted with DAPI. Images of fluorescent expression and implant targeting were taken using a Leica DM6 scanning microscope (Leica Microsystems) using a 10x objective.

Data Analysis

Behavioral Analysis

Overhead videos were collected (Teledyne FLIR, Chameleon 3) and animal positioning extracted via supervised deep learning networks[89]. Animal position information was transformed into freezing and interactions with ROI and bout features using BehaviorDEPOT software[90].

Fiber Photometry

Data were analyzed using a custom-written MATLAB pipeline. Raw recordings were downsampled 10x and the isosbestic signal was fit to the 465nm signal using the polyfit MATLAB function. Signals were transformed into z-scores for tone, freezing, and platform periods using a baseline of -5 to -4 seconds relative to event onset and smoothed with a 25 frame moving average. An animal's individual event responses were averaged to generate one trace per animal. Shock, avoid, and tone onset response z-scores were normalized across animals by using the mean response of the first tone period prior to shock delivery. Tone onset responses were calculated as the average value over the first 2 seconds of the tone. Shock/avoid responses were calculated as the average value over the 2 seconds following end of tone/shock. Platform and freezing responses were aligned to the onset or offset of the behavior. Average values of -2 to -1.5 seconds, -0.5 to 0 seconds, and +1.5 to +2 seconds from the event were used as baseline, event, and post-event responses, respectively. Baseline values were set to 0 to calculate the changes in DA preceding and following the event.

Behavioral Modeling

Time spent on the safety platform during conditioned tones was modeled using a Rescorla-Wagner model. We seeded the model with the amount of baseline time animals spent on the platform prior to shock. We reasoned the value of the platform would change as the animal learns the tone-shock association and as the animal learns the avoid-safety contingency.

We therefore updated the platform value based on failure (shock) trials. The value of the platform was calculated as:

$\Delta v_t = \alpha * (R_t - v_t)$, where:

- Δv_t is the change in associative strength of the platform at trial *t*
- α is the learning rate (free parameter)
- R_t is the outcome at trial *t*

- v_t is associative strength at time t (initially the baseline p(time on platform))

with the update rule:

$$\Delta v_t = \begin{cases} \alpha * (R_t - v_t) & \text{if success indicator at time t indicates = 0} \\ 0 & \text{otherwise} \end{cases}$$

This is fit by minimizing a loss function $MSE = (1 / N) * \Sigma_i (v_i - data_i)^2$, where:

- MSE is the mean squared error
- N is the # of data points
- v_i is the model's predicted value at trial i
- $data_i$ is the observed data at trial i

We also considered the alternative that success and failure trials both contribute to updating the platform value. We therefore implemented a model with two complementary learning rates (α): $\alpha_{failure}$, for learning from failure trials, and $\alpha_{success}$, for learning from successful avoid trials. Fit was performed as above. The value of the platform was calculated as:

$$\Delta v_t = \begin{cases} \alpha_{success} * (R_t - v_t) & \text{if trial outcome was a success,} \\ \alpha_{failure} * (R_t - v_t) & \text{if trial outcome was a failure} \end{cases}$$

Dopamine Modeling

Dopamine dynamics were modeled by individually fitting a temporal difference reinforcement learning model (Schultz e al., 1997) to DA signals from each task trial for PMA, FC, and Yoked-trained mice. This model assumes that dopamine signals encode prediction errors, reflecting discrepancies between expected and actual outcomes during fear conditions and avoidance learning. For each trial, a value function of the form:

$$V(t) = \beta(t) + b$$

Where β is a coefficient indexing the influence of *uncertainty* on the value of rewards, and b indexes the *baseline* measure of dopamine on a given trial at timestep t. The value function defines a time-dependent reward prediction based on uncertainty and expected value. The temporal difference (TD) error was computed as:

$$\delta(t) = S(t) + \gamma * V(t+1) - Vt$$

Where $S(t)$ is an external stimulus (shock/tone, modeled as binary),$V(t+1)$ is the predicted value at the subsequent timestep, and γ is the *discount* factor controlling the influence of future rewards on the current prediction. Dopamine signals were then modeled as

$$DA_{predicted}(t+1) = Vt + \alpha * \delta(t)$$

where α is the learning rate controlling the integration of TD errors into value predictions.

The TD model was fit to signals from each trial for each mouse using maximum likelihood estimation with the SciPy Optimize package in Python. Model error was calculated using a normalized root mean square error.

To facilitate comparison between the dynamics of different parameters across trials, optimized parameters for each subject were normalized between 0 and 1 across trials. To account for differences in numbers of given trial types between subjects, trials were grouped by trial outcome (shock or nonshock) and then averaged into thirds for early, middle, and late learning phases. To

assess change in parameter dynamics across learning, the difference from early learning was calculated.

Statistical analysis

Modeling was performed with custom Python code. All other statistical testing was performed in Graphpad Prism.

Data and code availability

Custom MATLAB and Python code available upon request.

Acknowledgements

We thank Dr. Peter Balsam for helpful discussions of this work. This work was supported by a Klingenstein-Simons Fellowship in Neuroscience, a Whitehall Foundation Research Grant and 1R01MH127214-01A1 (LAD), a Whitehall Foundation Research Grant and 1R01MH131858-01A1 (SAW), T32NS115753 and F31MH133387 (ZEZ) and T32NS115753 (TG).

Author Contributions

LAD, SAW, ZEZ, MFG and TG conceptualized the experiments. ZEZ, MFG and MS performed experiments. ZEZ and TG analyzed data. LAD, SAW and ZEZ wrote the manuscript. All authors edited the manuscript.

Declaration of Interests

The authors declare no competing interests.

During the preparation of this work the authors used the generative AI to check writing for grammar and clarity. After using this tool, the authors reviewed and edited the content as needed and take full responsibility for the content of the publication.

References

1. Pastor, V. & Medina, J. H. Medial prefrontal cortical control of reward- and aversion-based behavioral output: Bottom-up modulation. *European Journal of Neuroscience* **53**, 3039–3062 (2021).
2. Mair, R. G., Francoeur, M. J., Krell, E. M. & Gibson, B. M. Where Actions Meet Outcomes: Medial Prefrontal Cortex, Central Thalamus, and the Basal Ganglia. *Frontiers in Behavioral Neuroscience* **16**, (2022).
3. Matsumoto, K. & Tanaka, K. The role of the medial prefrontal cortex in achieving goals. *Current Opinion in Neurobiology* **14**, 178–185 (2004).
4. DeNardo, L. A. *et al.* Temporal evolution of cortical ensembles promoting remote memory retrieval. *Nature Neuroscience* **22**, 460–469 (2019).
5. Gabriel, C. J. *et al.* Transformations in prefrontal ensemble activity underlying rapid threat avoidance learning. *bioRxiv* 2024.08.28.610165 (2024) doi:10.1101/2024.08.28.610165.
6. Giustino, T. F. & Maren, S. The Role of the Medial Prefrontal Cortex in the Conditioning and Extinction of Fear. *Frontiers in Behavioral Neuroscience* **9**, 1–20 (2015).
7. Zeidler, Z. & DeNardo, L. The Role of Prefrontal Ensembles in Memory Across Time: Time-Dependent Transformations of Prefrontal Memory Ensembles. in *Engrams: A Window into the Memory Trace* (eds. Gräff, J. & Ramirez, S.) 67–78 (Springer International Publishing, Cham, 2024). doi:10.1007/978-3-031-62983-9_5.
8. Diehl, M. M., Bravo-Rivera, C. & Quirk, G. J. The study of active avoidance: A platform for discussion. *Neuroscience and Biobehavioral Reviews* **107**, 229–237 (2019).
9. Diehl, M. M. *et al.* Active avoidance requires inhibitory signaling in the rodent prelimbic prefrontal cortex. *eLife* (2018) doi:10.7554/eLife.34657.
10. Diehl, M. M. *et al.* Divergent projections of the prelimbic cortex bidirectionally regulate active avoidance. *eLife* **9**, 1–13 (2020).

11. Moscarello, J. M. & LeDoux, J. E. Active avoidance learning requires prefrontal suppression of amygdala-mediated defensive reactions. *Journal of Neuroscience* (2013) doi:10.1523/JNEUROSCI.2596-12.2013.
12. Jercog, D. *et al.* Dynamical prefrontal population coding during defensive behaviours. *Nature* **595**, 690–694 (2021).
13. Kajs, B. L., Loewke, A. C., Dorsch, J. M., Vinson, L. T. & Gunaydin, L. A. Divergent encoding of active avoidance behavior in corticostriatal and corticolimbic projections. *Scientific Reports* **12**, 1–11 (2022).
14. Bravo-Rivera, C., Roman-Ortiz, C., Brignoni-Perez, E., Sotres-Bayon, F. & Quirk, G. J. Neural Structures Mediating Expression and Extinction of Platform-Mediated Avoidance. *Journal of Neuroscience* (2014) doi:10.1523/JNEUROSCI.0191-14.2014.
15. Bravo-Rivera, C., Roman-Ortiz, C., Montesinos-Cartagena, M. & Quirk, G. J. Persistent active avoidance correlates with activity in prelimbic cortex and ventral striatum. *Frontiers in Behavioral Neuroscience* (2015) doi:10.3389/fnbeh.2015.00184.
16. Capuzzo, G. & Floresco, S. B. Prelimbic and Infralimbic Prefrontal Regulation of Active and Inhibitory Avoidance and Reward-Seeking. *Journal of Neuroscience* **40**, 4773–4787 (2020).
17. Weele, C. M. V., Siciliano, C. A. & Tye, K. M. Dopamine tunes prefrontal outputs to orchestrate aversive processing. *Brain Research* **1713**, 16–31 (2019).
18. Megan E. Fox & R. Mark Wightman. Contrasting Regulation of Catecholamine Neurotransmission in the Behaving Brain: Pharmacological Insights from an Electrochemical Perspective. *Pharmacol Rev* **69**, 12 (2017).
19. Aransay, A., Rodríguez-López, C., García-Amado, M., Clascá, F. & Prensa, L. Long-range projection neurons of the mouse ventral tegmental area: a single-cell axon tracing analysis. *Front. Neuroanat.* **9**, (2015).
20. Abe, K. *et al.* Functional diversity of dopamine axons in prefrontal cortex during classical conditioning. *eLife* **12**, RP91136 (2024).

649 21. Islam, K. U. S., Meli, N. & Blaess, S. The Development of the Mesoprefrontal Dopaminergic
650 System in Health and Disease. *Front. Neural Circuits* **15**, (2021).
651 22. Thierry, A. M., Stinus, L., Blanc, G. & Glowinski, J. Some evidence for the existence of
652 dopaminergic neurons in the rat cortex. *Brain Res* **50**, 230–234 (1973).
653 23. Ikemoto, S. Brain reward circuitry beyond the mesolimbic dopamine system: A
654 neurobiological theory. *Neuroscience & Biobehavioral Reviews* **35**, 129–150 (2010).
655 24. Lammel, S. *et al.* Unique Properties of Mesoprefrontal Neurons within a Dual
656 Mesocorticolimbic Dopamine System. *Neuron* **57**, 760–773 (2008).
657 25. Chiodo, L. A., Bannon, M. J., Grace, A. A., Roth, R. H. & Bunney, B. S. Evidence for the
658 absence of impulse-regulating somatodendritic and synthesis-modulating nerve terminal
659 autoreceptors on subpopulations of mesocortical dopamine neurons. *Neuroscience* **12**, 1–16
660 (1984).
661 26. M J Bannon & R H Roth. Pharmacology of mesocortical dopamine neurons. *Pharmacol Rev*
662 **35**, 53 (1983).
663 27. Björklund, A. & Dunnett, S. B. Dopamine neuron systems in the brain: an update. *Trends in*
664 *Neurosciences* **30**, 194–202 (2007).
665 28. Lammel, S., Ion, D. I., Roeper, J. & Malenka, R. C. Projection-Specific Modulation of
666 Dopamine Neuron Synapses by Aversive and Rewarding Stimuli. *Neuron* **70**, 855–862
667 (2011).
668 29. Lammel, S. *et al.* Input-specific control of reward and aversion in the ventral tegmental area.
669 *Nature* **491**, 212–217 (2012).
670 30. Kim, C. K. *et al.* Simultaneous fast measurement of circuit dynamics at multiple sites across
671 the mammalian brain. *Nature methods* **13**, 325–328 (2016).
672 31. Vander Weele, C. M. *et al.* Dopamine enhances signal-to-noise ratio in cortical-brainstem
673 encoding of aversive stimuli. *Nature* **563**, 397–401 (2018).
674 32. Abercrombie, E. D., Keefe, K. A., DiFrischia, D. S. & Zigmond, M. J. Differential Effect of

675 Stress on In Vivo Dopamine Release in Striatum, Nucleus Accumbens, and Medial Frontal
676 Cortex. *Journal of Neurochemistry* **52**, 1655–1658 (1989).
677 33. Lerner, T. N., Holloway, A. L. & Seiler, J. L. Dopamine, Updated: Reward Prediction Error and
678 Beyond. *Current Opinion in Neurobiology* **67**, 123–130 (2021).
679 34. Arco, A. D., Park, J. & Moghaddam, B. Unanticipated Stressful and Rewarding Experiences
680 Engage the Same Prefrontal Cortex and Ventral Tegmental Area Neuronal Populations.
681 *eNeuro* **7**, (2020).
682 35. Zafiri, D. & Duvarci, S. Dopaminergic circuits underlying associative aversive learning. *Front.*
683 *Behav. Neurosci.* **16**, (2022).
684 36. Pezze, M. A., Bast, T. & Feldon, J. Significance of dopamine transmission in the rat medial
685 prefrontal cortex for conditioned fear. *Cereb Cortex* **13**, 371–380 (2003).
686 37. Vergara, M. D., Keller, V. N., Fuentealba, J. A. & Gysling, K. Activation of type 4 dopaminergic
687 receptors in the prelimbic area of medial prefrontal cortex is necessary for the expression of
688 innate fear behavior. *Behavioural Brain Research* **324**, 130–137 (2017).
689 38. Díaz, F. C., Kramar, C. P., Hernandez, M. A. & Medina, J. H. Activation of D1/5 Dopamine
690 Receptors in the Dorsal Medial Prefrontal Cortex Promotes Incubated-Like Aversive
691 Responses. *Frontiers in Behavioral Neuroscience* **11**, 209 (2017).
692 39. Fibiger, H. C., Zis, A. P. & Phillips, A. G. Haloperidol-induced disruption of conditioned
693 avoidance responding: attenuation by prior training or by anticholinergic drugs. *Eur J*
694 *Pharmacol* **30**, 309–314 (1975).
695 40. Arnt, J. Pharmacological Specificity of Conditioned Avoidance Response Inhibition in Rats:
696 Inhibition by Neuroleptics and Correlation to Dopamine Receptor Blockade. *Acta*
697 *Pharmacologica et Toxicologica* **51**, 321–329 (1982).
698 41. Wadenberg, M.-L., Ericson, E., Magnusson, O. & Ahlenius, S. Suppression of conditioned
699 avoidance behavior by the local application of (−)sulpiride into the ventral, but not the dorsal,

striatum of the rat. *Biological Psychiatry* **28**, 297–307 (1990).

42. Stark, H., Bischof, A. & Scheich, H. Increase of extracellular dopamine in prefrontal cortex of gerbils during acquisition of the avoidance strategy in the shuttle-box. *Neurosci Lett* **264**, 77–80 (1999).
43. Rescorla, R. A. & Wagner, A. A theory of Pavlovian conditioning: Variations in the effectiveness of reinforcement and nonreinforcement. in *Classical Conditioning II: Current Research and Theory* 64–99 (Appleton-Century-Crofts, 1972).
44. Yau, J. O.-Y. & McNally, G. P. The Rescorla-Wagner model, prediction error, and fear learning. *Neurobiology of Learning and Memory* **203**, 107799 (2023).
45. Sun, F. *et al.* Next-generation GRAB sensors for monitoring dopaminergic activity in vivo. *Nature Methods* **17**, 1156–1166 (2020).
46. Sorg, B. A. & Kalivas, P. W. Effects of cocaine and footshock stress on extracellular dopamine levels in the medial prefrontal cortex. *Neuroscience* **53**, 695–703 (1993).
47. Gunaydin, L. A. *et al.* Natural neural projection dynamics underlying social behavior. *Cell* **157**, 1535–1551 (2014).
48. Mantz, J., Thierry, A. M. & Glowinski, J. Effect of noxious tail pinch on the discharge rate of mesocortical and mesolimbic dopamine neurons: selective activation of the mesocortical system. *Brain Research* **476**, 377–381 (1989).
49. THIERRY, A. M., TASSIN, J. P., BLANC, G. & GLOWINSKI, J. Selective activation of the mesocortical DA system by stress. *Nature* **263**, 242–244 (1976).
50. Sullivan, R. M. & Gratton, A. Relationships between stress-induced increases in medial prefrontal cortical dopamine and plasma corticosterone levels in rats: role of cerebral laterality. *Neuroscience* **83**, 81–91 (1998).
51. Feenstra, M. G. P., Teske, G., Botterblom, M. H. A. & De Bruin, J. P. C. Dopamine and noradrenaline release in the prefrontal cortex of rats during classical aversive and appetitive

conditioning to a contextual stimulus: Interference by novelty effects. *Neuroscience Letters* (1999) doi:10.1016/S0304-3940(99)00601-1.

52. Wilkinson, L. S. *et al.* Dissociations in dopamine release in medial prefrontal cortex and ventral striatum during the acquisition and extinction of classical aversive conditioning in the rat. *European Journal of Neuroscience* **10**, 1019–1026 (1998).
53. Feenstra, M. G. P. Dopamine and noradrenaline release in the prefrontal cortex in relation to unconditioned and conditioned stress and reward. in *Progress in Brain Research* vol. 126 133–163 (Elsevier, 2000).
54. Feenstra, M. G. P., Vogel, M., Botterblom, M. H. A., Joosten, R. N. J. M. A. & De Bruin, J. P. C. Dopamine and noradrenaline efflux in the rat prefrontal cortex after classical aversive conditioning to an auditory cue. *European Journal of Neuroscience* **13**, 1051–1054 (2001).
55. Pezze, M. A., Marshall, H. J., Domonkos, A. & Cassaday, H. J. Effects of dopamine D1 modulation of the anterior cingulate cortex in a fear conditioning procedure. *Progress in Neuro-Psychopharmacology and Biological Psychiatry* **65**, 60–67 (2016).
56. Simon, N. W. & Moghaddam, B. Neural processing of reward in adolescent rodents. *Dev Cogn Neurosci* **11**, 145–154 (2015).
57. Alexander, W. H. & Brown, J. W. Medial prefrontal cortex as an action-outcome predictor. *Nat Neurosci* **14**, 1338–1344 (2011).
58. Matsumoto, M., Matsumoto, K., Abe, H. & Tanaka, K. Medial prefrontal cell activity signaling prediction errors of action values. *Nat Neurosci* **10**, 647–656 (2007).
59. Lauzon, N. M., Bechard, M., Ahmad, T. & Laviolette, S. R. Supra-normal stimulation of dopamine D1 receptors in the prelimbic cortex blocks behavioral expression of both aversive and rewarding associative memories through a cyclic-AMP-dependent signaling pathway. *Neuropharmacology* **67**, 104–114 (2013).
60. Ellwood, I. T. *et al.* Tonic or Phasic Stimulation of Dopaminergic Projections to Prefrontal Cortex Causes Mice to Maintain or Deviate from Previously Learned Behavioral Strategies.

751 *J. Neurosci.* **37**, 8315 (2017).

752 61. Fadda, F. *et al.* Stress-induced increase in 3,4-dihydroxyphenylacetic acid (DOPAC) levels in
753 the cerebral cortex and in n. accumbens: Reversal by diazepam. *Life Sciences* **23**, 2219–
754 2224 (1978).

755 62. Luo, R. *et al.* A dopaminergic switch for fear to safety transitions. *Nature Communications* **9**,
756 1–11 (2018).

757 63. Hitora-Imamura, N. *et al.* Prefrontal dopamine regulates fear reinstatement through the
758 downregulation of extinction circuits. *eLife* **4**, e08274 (2015).

759 64. Pfeiffer, U. J. & Fendt, M. Prefrontal dopamine D4 receptors are involved in encoding fear
760 extinction. *NeuroReport* **17**, 847–850 (2006).

761 65. Zbukvic, I. C., Park, C. H. J., Ganella, D. E., Lawrence, A. J. & Kim, J. H. Prefrontal
762 Dopaminergic Mechanisms of Extinction in Adolescence Compared to Adulthood in Rats.
763 *Front. Behav. Neurosci.* **11**, (2017).

764 66. Sartori, S. B. *et al.* Fear extinction rescuing effects of dopamine and L-DOPA in the
765 ventromedial prefrontal cortex. *Transl Psychiatry* **14**, 11 (2024).

766 67. Corcoran, K. A. & Quirk, G. J. Activity in prelimbic cortex is necessary for the expression of
767 learned, but not innate, fears. *Journal of Neuroscience* **27**, 840–844 (2007).

768 68. Vander Weele, C. M., Siciliano, C. A. & Tye, K. M. Dopamine tunes prefrontal outputs to
769 orchestrate aversive processing. *Brain Res* **1713**, 16–31 (2019).

770 69. Miller, E. K. & Cohen, J. D. AN INTEGRATIVE THEORY OF PREFRONTAL CORTEX
771 FUNCTION. *Annual Review of Neuroscience* **24**, 167–202 (2001).

772 70. Ott, T. & Nieder, A. Dopamine and Cognitive Control in Prefrontal Cortex. *Trends in Cognitive*
773 *Sciences* **23**, 213–234 (2019).

774 71. Baeg, E. H. *et al.* Fast Spiking and Regular Spiking Neural Correlates of Fear Conditioning in
775 the Medial Prefrontal Cortex of the Rat. *Cerebral Cortex* **11**, 441–451 (2001).

776 72. Jacobs, D. S. & Moghaddam, B. Prefrontal Cortex Representation of Learning of Punishment

Probability During Reward-Motivated Actions. *The Journal of Neuroscience* **40**, 5063–5077 (2020).

73. Davis, J. F. *et al.* Lesions of the Medial Prefrontal Cortex Cause Maladaptive Sexual Behavior in Male Rats. *Biological Psychiatry* **67**, 1199–1204 (2010).
74. Lesting, J. *et al.* Patterns of Coupled Theta Activity in Amygdala-Hippocampal-Prefrontal Cortical Circuits during Fear Extinction. *PLOS ONE* **6**, e21714 (2011).
75. Otani, S., Bai, J. & Blot, K. Dopaminergic modulation of synaptic plasticity in rat prefrontal neurons. *Neurosci. Bull.* **31**, 183–190 (2015).
76. Buchta, W. C., Mahler, S. V., Harlan, B., Aston-Jones, G. S. & Riegel, A. C. Dopamine terminals from the ventral tegmental area gate intrinsic inhibition in the prefrontal cortex. *Physiological Reports* **5**, e13198 (2017).
77. Chen, G., Greengard, P. & Yan, Z. Potentiation of NMDA receptor currents by dopamine D1 receptors in prefrontal cortex. *Proc Natl Acad Sci U S A* **101**, 2596–2600 (2004).
78. Anastasiades, P. G., Boada, C. & Carter, A. G. Cell-Type-Specific D1 Dopamine Receptor Modulation of Projection Neurons and Interneurons in the Prefrontal Cortex. *Cereb Cortex* **29**, 3224–3242 (2019).
79. Tritsch, N. X. & Sabatini, B. L. Dopaminergic modulation of synaptic transmission in cortex and striatum. *Neuron* **76**, 33–50 (2012).
80. Gee, S. *et al.* Synaptic activity unmasks dopamine D2 receptor modulation of a specific class of layer V pyramidal neurons in prefrontal cortex. *J Neurosci* **32**, 4959–4971 (2012).
81. Anastasiades, P. G. & Carter, A. G. Circuit organization of the rodent medial prefrontal cortex. *Trends Neurosci* **44**, 550–563 (2021).
82. Han, S.-W., Kim, Y.-C. & Narayanan, N. S. Projection targets of medial frontal D1DR-expressing neurons. *Neuroscience Letters* **655**, 166–171 (2017).
83. Gongwer, M. W. *et al.* Brain-Wide Projections and Differential Encoding of Prefrontal Neuronal Classes Underlying Learned and Innate Threat Avoidance. *J. Neurosci.* **43**, 5810–5830

(2023).

84. Mongia, S. *et al.* The Ventral Tegmental Area has calbindin neurons with the capability to co-release glutamate and dopamine into the nucleus accumbens. *Eur J Neurosci* **50**, 3968–3984 (2019).

85. Lavin, A. *et al.* Mesocortical Dopamine Neurons Operate in Distinct Temporal Domains Using Multimodal Signaling. *J. Neurosci.* **25**, 5013–5023 (2005).

86. Kumar, M., Green, S. M. & Urs, N. M. Role of Cortical Dopamine circuits in regulating Striatal Dopamine dynamics during Reversal Learning. *The FASEB Journal* **36**, (2022).

87. LeDoux, J. & Daw, N. D. Surviving threats: neural circuit and computational implications of a new taxonomy of defensive behaviour. *Nature Reviews Neuroscience* **19**, 269–282 (2018).

88. Anne E. Urai *et al.* Citric Acid Water as an Alternative to Water Restriction for High-Yield Mouse Behavior. *eNeuro* **8**, ENEURO.0230-20.2020 (2021).

89. Mathis, A. *et al.* DeepLabCut: markerless pose estimation of user-defined body parts with deep learning. *Nature Neuroscience* **21**, 1281–1289 (2018).

90. Gabriel, C. J. *et al.* Behavior DEPOT is a simple, flexible tool for automated behavioral detection based on marker less pose tracking. *eLife* **11**, 1–33 (2022).

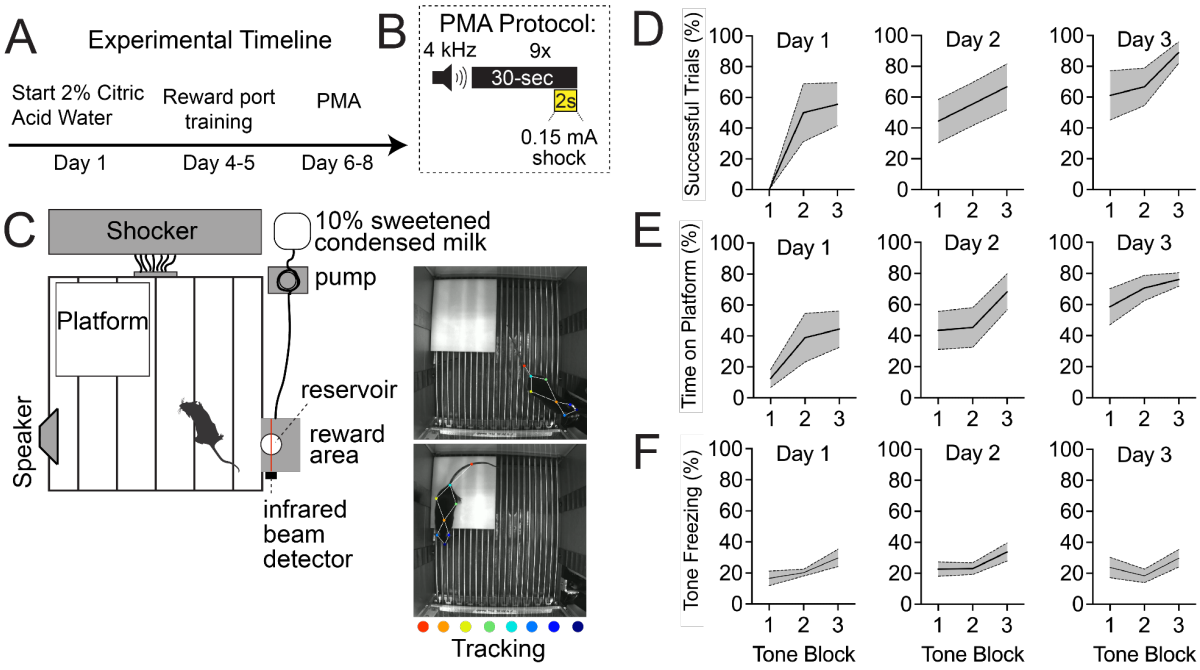

Figure 1. Mice learn avoidance contingencies and tone-shock relationships in platform mediated avoidance (PMA) assay.
A. Experimental timeline.
B. Behavioral training protocol.
C. Schematic of PMA chamber (left) and frames from videos (right).
D-F. Behavior across 3 days of PMA. On each day, data is analyzed in bins of 3 tones.
D. Successful trials ($F_{Trial}(1.27,6.34)=17.99$, $p=0.004$; $F_{Day}(1.96,9.79)=7.64$, $p=0.01$; n=6 mice).
E. Time on platform during tones ($F_{Trial}(1.37,6.82)=21.03$, $p=0.002$; $F_{Day}(1.74,8.71)=8.24$, $p=0.01$; n=6 mice).
F. Freezing during tones ($F_{Trial}(1.72,8.61)=1.31$, $p=0.31$; $F_{Day}(1.38,6.9)=1.83$, $p=0.22$; n=6 mice).

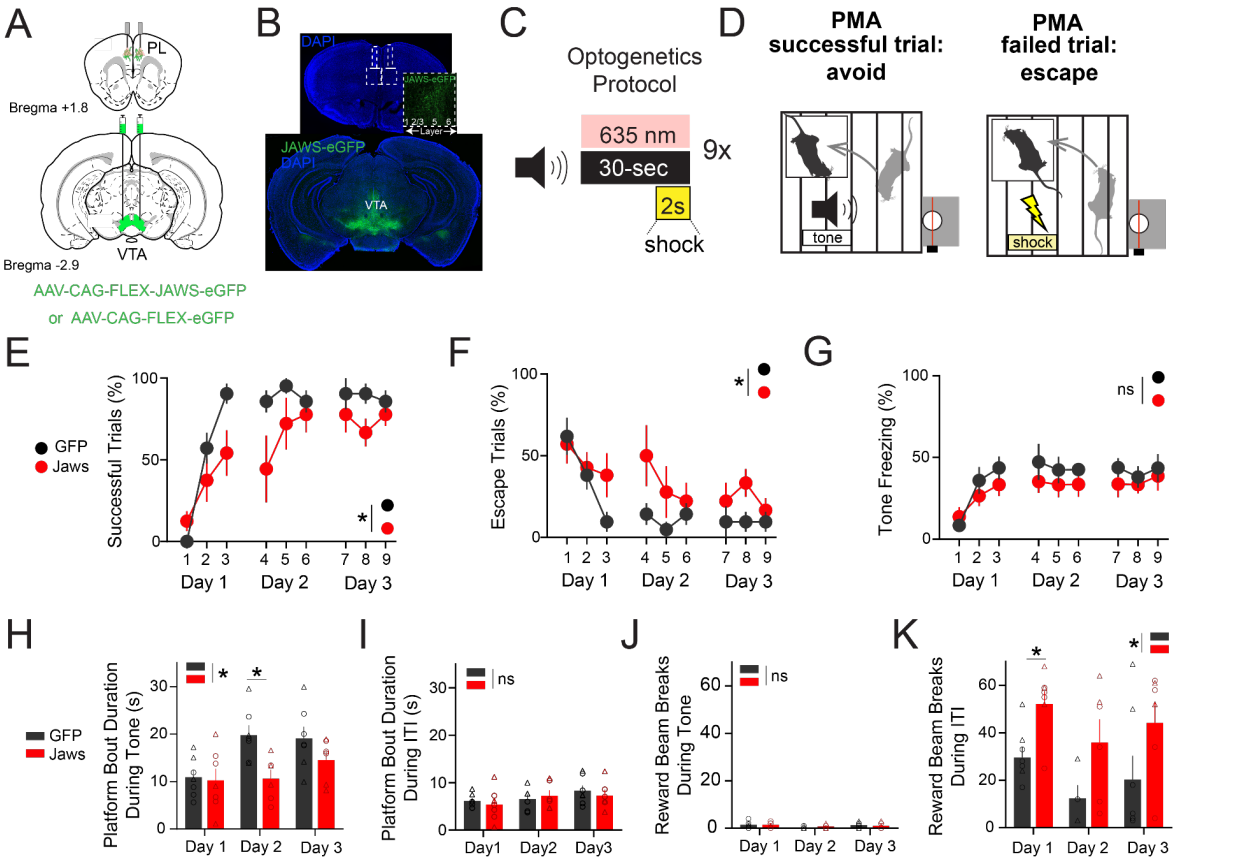

Figure 2. Optogenetic inhibition of DAergic axon terminals in mPFC impairs avoidance contingency learning but not tone-shock learning.

A. Schematic of viral and fiberoptic targeting locations.

B. Coronal sections from a representative brain showing Jaws-eGFP expression in VTA and bilateral fiber placement in PL.

C. Optogenetic inhibition during PMA. 635nm laser light was presented coincidently with a 30 second 4kHz tone that co-terminated with a 2-second footshock.

D. Schematics showing a successful trial when mice preemptively avoided the shock vs. an escape trial when mice leaped to the platform after shock begins.

E. Percent successful trials across days in GFP vs. Jaws mice ($F_{time}(4.26, 49) = 17$, $P<0.0001$; $F_{opsin}(1, 13) = 5.66$, $p=0.03$; $F_{interaction}(8, 92) = 2.197$, $p=0.06$).

F. Percent escape trials across days in GFP vs. Jaws mice (F_{time} (4,43, 49.86) = 5.43, $p=0.0007$; F_{opsin} (1, 13) = 4.78, $p=0.04$; $F_{interaction}$ (8, 90) = 1.04; $p=0.4$).

G. Percent time freezing during tone across days in GFP vs. Jaws mice (F_{time} (4.32, 46.98) = 8.41, $P<0.0001$; F_{opsin} (1, 12) = 1.4, $p=0.2$; $F_{interaction}$ (8, 87) = 1.01; $p=0.4$).

H. Platform bout duration during tone periods across days in GFP vs Jaws mice ($F_{time}(4.26, 49) = 17$, $p=0.005$; $F_{opsin}(1, 13) = 5.66$, $p=0.04$; $F_{interaction}(8, 92) = 2.197$, $p=0.06$; GFP vs. Jaws Day 1 p = 0.9, Day 2 = 0.02, Day 3 = 0.4.

I. Platform bout duration during ITI (inter-trial interval) across days in GFP vs. Jaws mice ($F_{time}(1.75, 18.43) = 3.4$, $p=0.057$; $F_{opsin}(1, 12) = 0.8$, $p=0.7$; $F_{interaction}(2, 21) = 0.67$, $p=0.5$).

J. Number of reward beam breaks during the tone period across days in GFP and Jaws mice ($F_{time}(1.9, 32.1) = 2.5$, $p=0.09$; $F_{opsin}(1, 33) = 5.66$, $p=0.9$; $F_{interaction}(2, 33) = 0.2$, $p=0.7$). E-K statistical testing performed with a mixed effects model, n=7 GFP, n=7-8 Jaws.

K. Number of reward beam breaks during ITI across days in GFP and Jaws mice ($F_{time}(1.9, 20.1) = 4.3$, $p=0.02$; $F_{opsin}(1, 12) = 8.2$, $p=0.01$; $F_{interaction}(2, 21) = 0.02$, $p=0.98$; GFP vs Jaws Day 1 $p=0.02$; Day 2 $p=0.2$; Day 3 $p=0.3$).
Triangles represent males and circles represent females.
*P<0.05,. Graphs represent mean ± SEM.

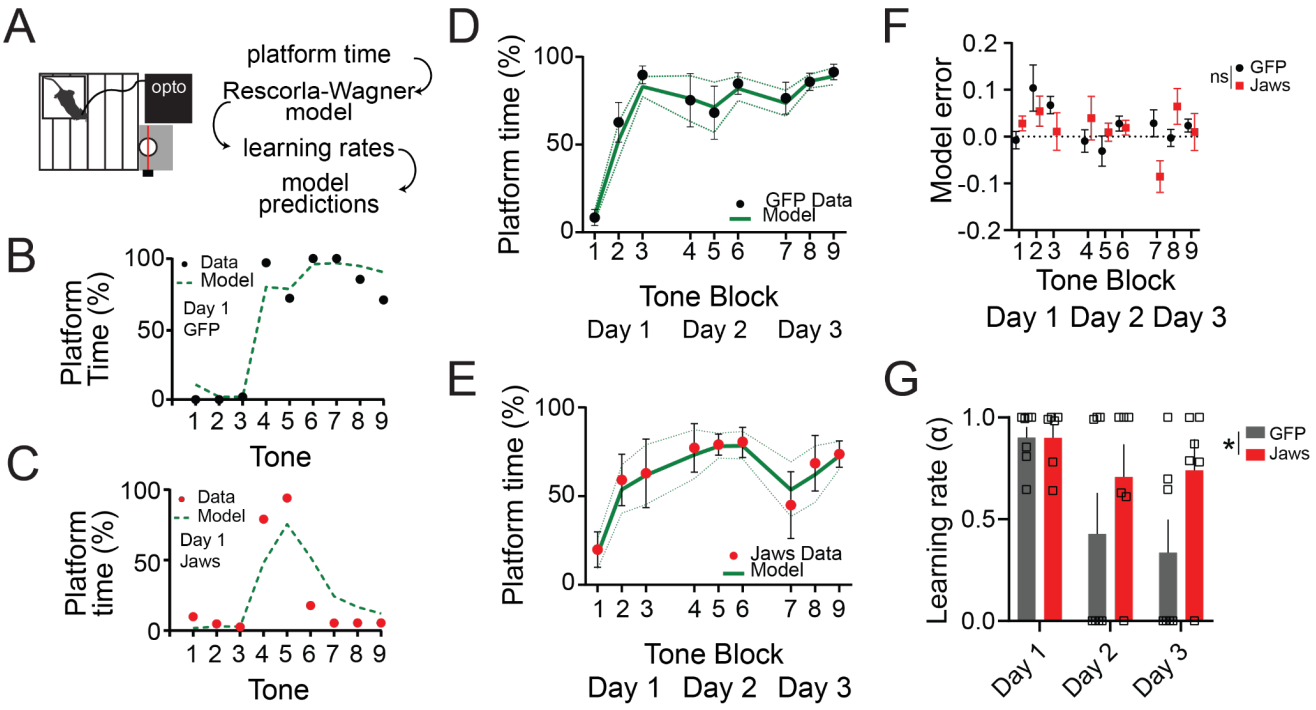

Figure 3. Inhibition of mPFC DA release decreases learning rates during PMA.
A. Schematic of optogenetic experiment and modeling approach.
B. Example model performance for a GFP-expressing animal.
C. Same as B for a Jaws-expressing animal.
D. Percent time on platform during the tone for GFP-expressing animals, both observed and model predictions.
E. Same as D for Jaws-expressing animals.
F. Quantification of modeling prediction error reveals no difference in the model's performance between GFP and Jaws groups. Mixed effects model ($F_{time}(3.32, 39.87)=2.1$, $p=0.1$; $F_{opsin}(1, 96)=0.69$, $p=0.6$; $F_{interaction}(8, 96)=2$, $p=0.052$).
G. Model-derived learning rates for GFP vs. Jaws animals. Two-way ANOVA ($F_{time}(1.4, 15.8)=3.2$, $p=0.07$; $F_{opsin}(1, 11)=5.4$, $p=0.04$; $F_{interaction}(2, 22)=0.8$, $p=0.4$).

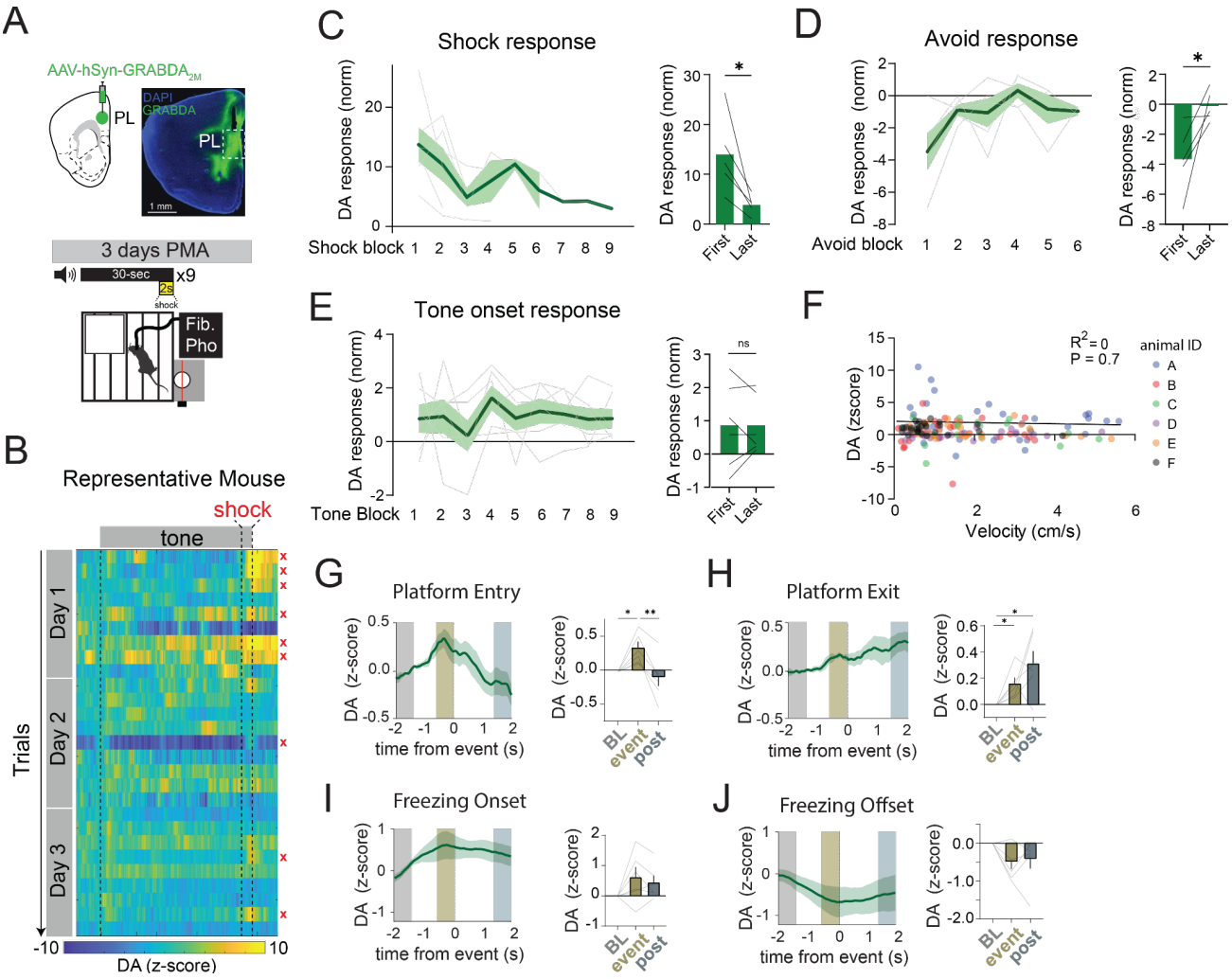

Figure 4. mPFC DA dynamics during PMA

A. Representative coronal section showing AAV-GRAB_DA$_{2m}$ expression and fiber placement. **B.** Heatmap showing z-scored DA fluorescence in a representative mouse. Red x marks shock trials.

C. DA signal decreases following repeated shocks. First block vs last block paired t-test p=0.03.

D. DA signal increases following repeated avoids. First block vs last block paired t-test p=0.04.

E. DA dynamics in response to tone onset do not show overt dynamics. First block vs last block paired t-test p=0.9.

F. Velocity does not correlate with DA fluorescence. Data points are color coded by animal, with the average DA response and velocity at the start (first 3 seconds) of each tone. Pearson's R^2 = 0, p=0.7.

G-J. DA dynamics surrounding avoidance and freezing behavior at baseline (BL), immediately preceding the behavior (event), or after the behavior (post).

G. DA ramps up prior to platform entry then back down following platform entry. Repeated measures one-way ANOVA F(10), p = 0.01. BL vs. event p = 0.02. Event vs. post p=0.007. BL vs. post p= 0.7.

H. DA dynamics ramp up during platform exit. Repeated measures one-way ANOVA F=6, p=0.04. BL vs. event p=0.03. Event vs. post p=0.4. BL vs. post p = 0.04.

I. DA dynamics during freezing onset. Repeated measures one-way ANOVA F=2.8, p=0.1.

J. DA dynamics during freezing offset. Repeated measures one-way ANOVA F=3.1, p=0.1.

N=6 animals. Posthoc testing performed with Tukey's test.

*P<0.05, ** P<0.01. Graphs represent mean ± SEM.

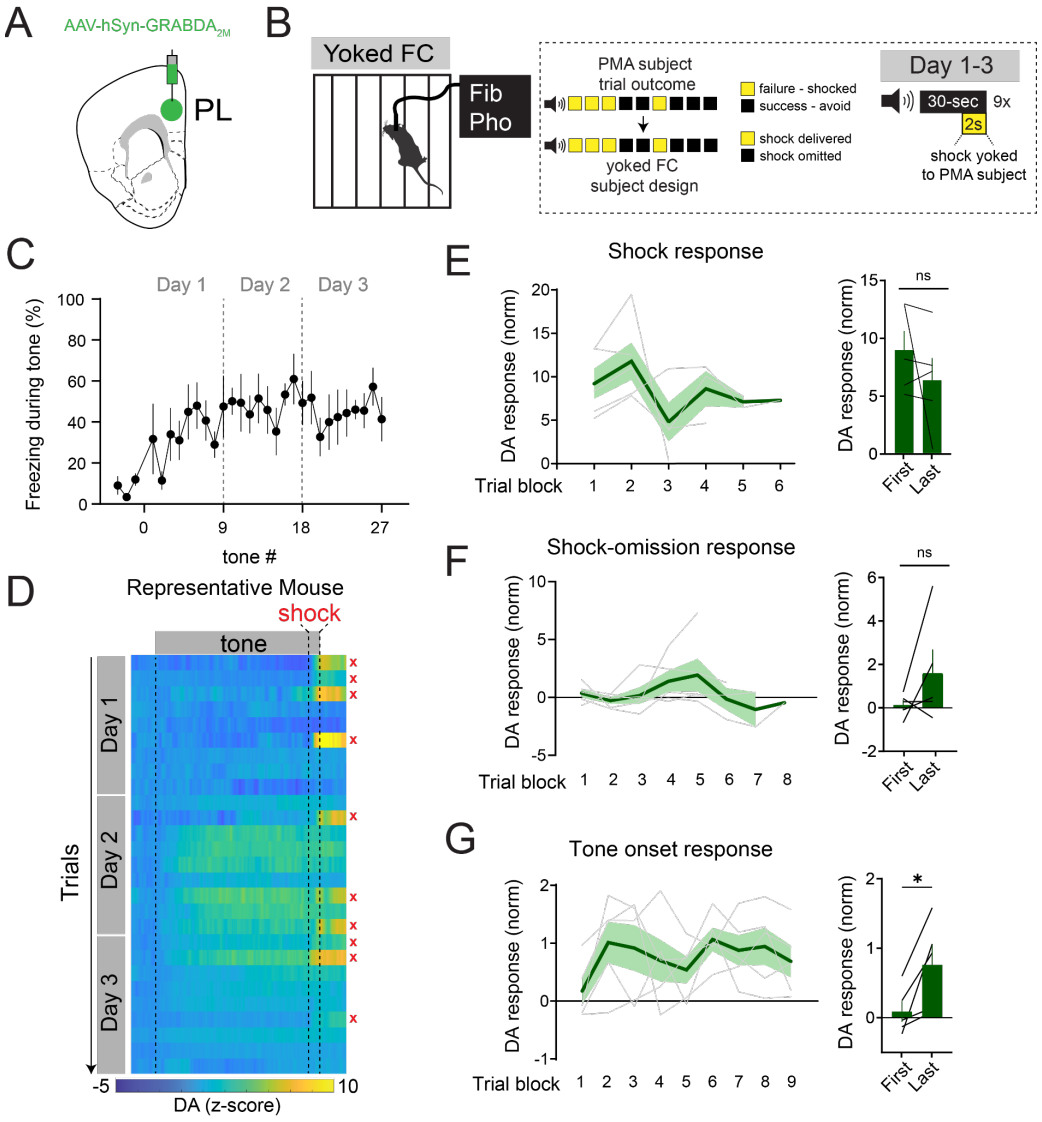

Figure 5. Removing the avoidance contingency from PMA alters mPFC DA representations of trial outcomes and cues.

A. Schematic showing GRABDA recording in prelimbic (PL) cortex.
B. Experimental design: animals were placed in a fear conditioning (FC) arena and exposed to tones. Presence of a co-terminal shock was dependent on the matched trial outcome of a subject from PMA.
C. Heatmap of GRABDA fluoresence (zscored) from representative mouse.
D. Freezing during the tone across days.
E. Left: DA levels to shock across time. Right: Comparison of first to last shock response block. Two-tailed paired t-test p=0.3.
F. Left: DA levels to shock-omission across time. Right: Comparison of first to last shock omission block. Paired t-test p=0.2.

G. Left: DA levels to tone onset across time. Right: Comparison of first to last tone block onset. Paired t-test p=0.03. *p<0.05.

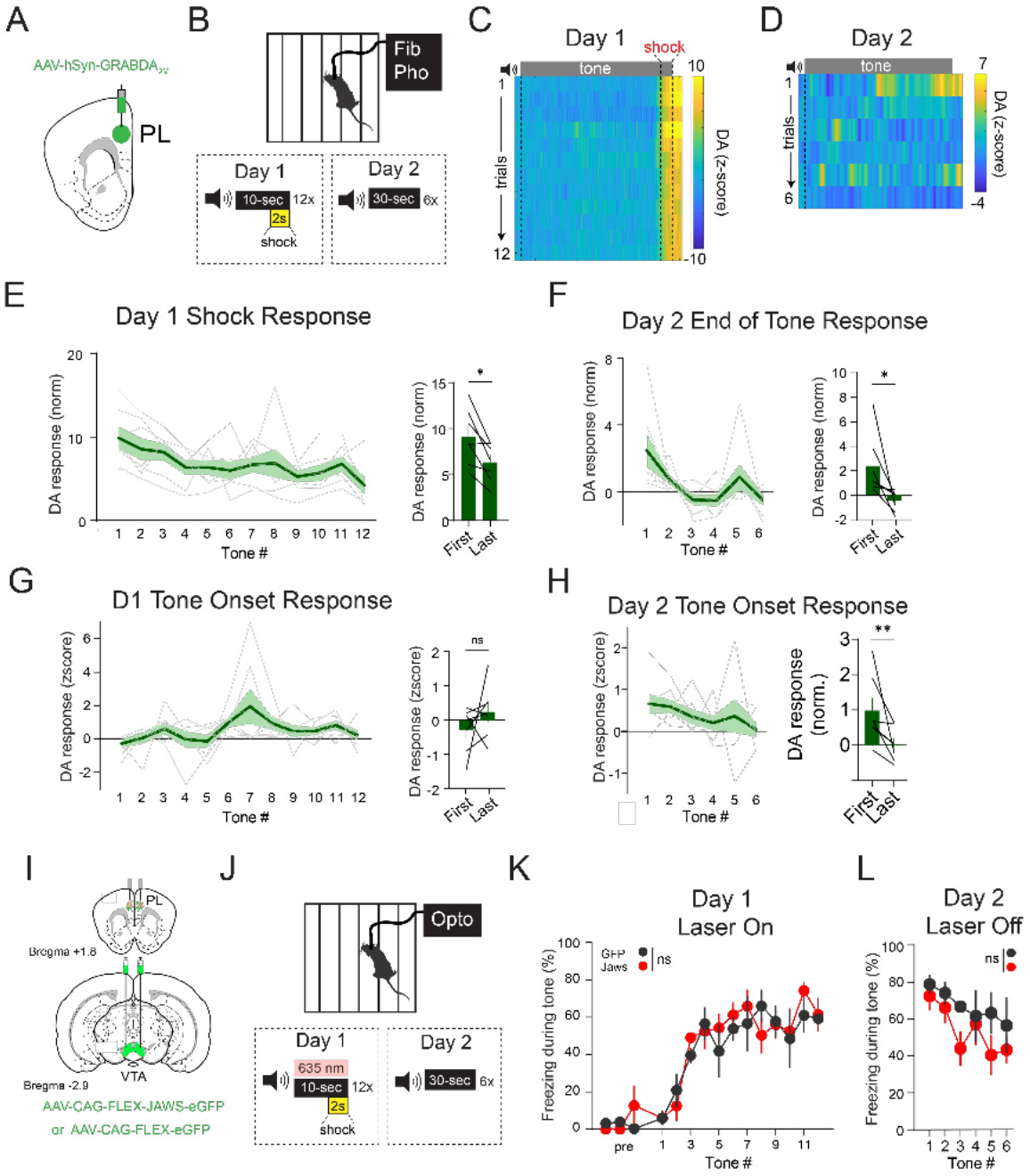

Figure 6. mPFC DA reflects but is not required for cued fear conditioning.
A. AAV and fiber placement GRABDA fiber photometry.
B. Experimental design.
C. Heatmap from representative mouse showing GRABDA fluorescence during fear conditioning. and
D. retrieval.
E. DA levels to shock during fear conditioning decrease across time. (right) Comparison of first to last shock response. Two-tailed paired t-test p=0.01.
F. DA levels during end of tone during the expected footshock on retrieval day. (right) Comparison of first and last tone response. Two-tailed paired t-test p=0.03.
G. DA levels during tone onset during fear conditioning do not linearly change across time. (right) Comparison of first and last tone response. Two-tailed paired t-test p=0.3.

H. DA levels during tone onset during fear memory retrieval decrease across time. (right) Comparison of first and last tone response. Two-tailed paired t-test p=0.008. * P<0.05, ** P<0.01, ns P>0.05 **.**
I. AAV injection and fiber placement for optogenetic inhibition of VTA-mPFC axon terminals.
J. Experimental protocol.
K. Freezing during fear conditioning did not differ between GFP and Jaws groups. Two-way repeated measures ANOVA (F_{time} (4.7, 33.3)=18.2, P<0.001; F_{opsin} (1, 7)=0.6, p=0.4; $F_{interaction}$ (14, 98)=0.5, p=0.9).
L. Freezing during fear memory retrieval did not differ between GFP and Jaws groups. Two-way RM ANOVA (F_{time} (2.8, 20.2)=5.5, p=0.006; F_{opsin} (1, 7)=1.2, p=0.2; $F_{interaction}$ (5, 35)=0.8, p=0.5).

819

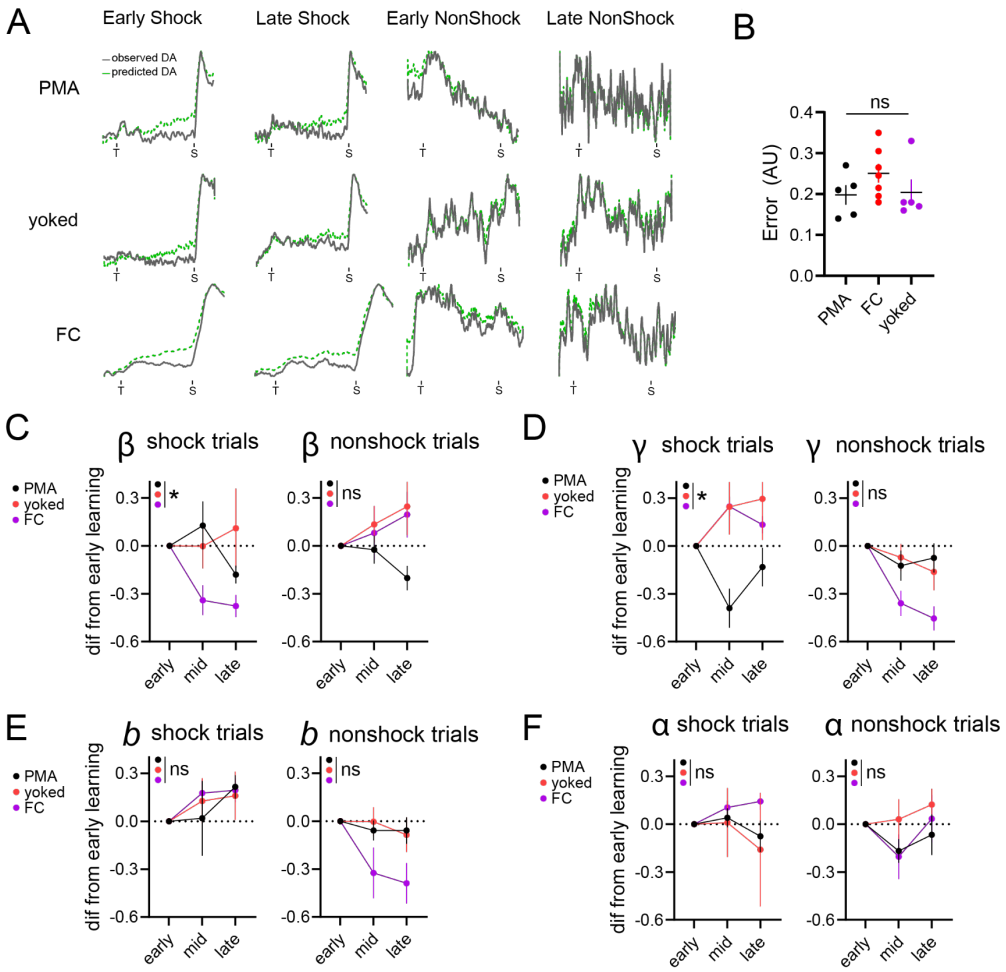

Figure 7. Temporal difference model captures assay-specific dynamics governing mPFC DA.
A. Representative observed versus model predicted DA responses across assay and learning. Y-axis scaled to min and max values for each trace. X axis tick marks indicate tone onset (T) and shock/shock omission onset (S).
B. The model has a similar error rate across assays. One-way ANOVA F=1.3, p = 0.29.
C. Temporal scaling factor (β) in (left) shock and (right) nonshock trials, averaged into values during early, middle, and late trials. (left) Two-way ANOVA $F_{time}(2,30)=1.9$, p=0.1, $F_{assay}(2,15)=4.1$, p=0.03, $F_{time\ x\ assay}(4,30)=3.1$, p=0.02. Mid PMA vs FC p=0.006, Late yoked vs FC p=0.006. (right) Two-way ANOVA $F_{time}(2,28)=1.4$, p=0.5, $F_{assay}(2,14)=1.5$, p=0.2, $F_{time\ x\ assay}(4,28)=5.5$, p=0.2.
D. Same as C for future discounting factor (γ). Two-way ANOVA $F_{time}(2,30)=1.1$, p=0.3, $F_{assay}(2,15)=5$, p=0.02, $F_{time\ x\ assay}(4,30)=5.2$, p=0.002. Mid PMA vs FC p=0.0002, Mid PMA vs yoked p=0.0007, Late PMA vs yoked p=0.02. (right) Two-way ANOVA $F_{time}(2,28)=9$, p=0.0009, $F_{assay}(2,14)=7.1$, p=0.007, $F_{time\ x\ assay}(4,28)=2.5$, p=0.059.
E. Same as C for base parameter (b). Two-way ANOVA $F_{time}(2,30)=3.1$, p=0.056, $F_{assay}(2,15)=0.1$, p=0.9, $F_{time\ x\ assay}(4,30)=0.3$, p=0.8. (right) Two-way ANOVA $F_{time}(2,28)=3.8$, p=0.03, $F_{assay}(2,14)=2.7$, p=0.1, $F_{time\ x\ assay}(4,28)=1.8$, p=0.15.
F. Same as C for learning rate parameter (α). Two-way ANOVA $F_{time}(2,30)=0.5$, p=0.6, $F_{assay}(2,15)=0.5$, p=0.5, $F_{time\ x\ assay}(4,30)=0.6$, p=0.6. (right) Two-way ANOVA $F_{time}(2,28)=2$, p=0.1, $F_{assay}(2,14)=0.7$, p=0.4, $F_{time\ x\ assay}(4,28)=0.6$, p=0.6.

Supplemental Figures

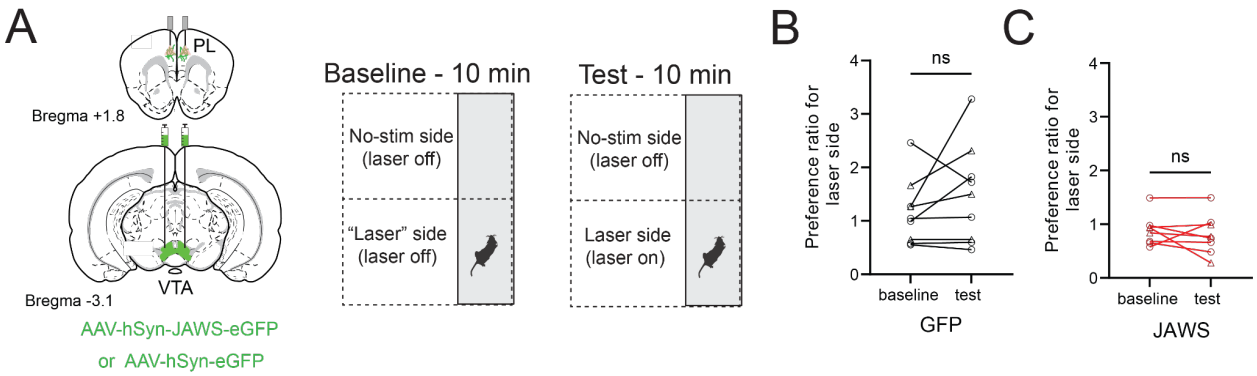

Figure S1. Inhibition of VTA DA terminals in mPFC does not cause real-time place avoidance.
A. Surgical strategy and schematic of real-time place preference assay.
B. Animal preference for "laser" side of the arena during baseline (laser off) period and during testing (laser on) period in GFP-expressing animals. Paired t-test, p=0.2, n=9.
C. Same as B. for Jaws-expressing animals. Paired t-test, p=0.4, n=8.

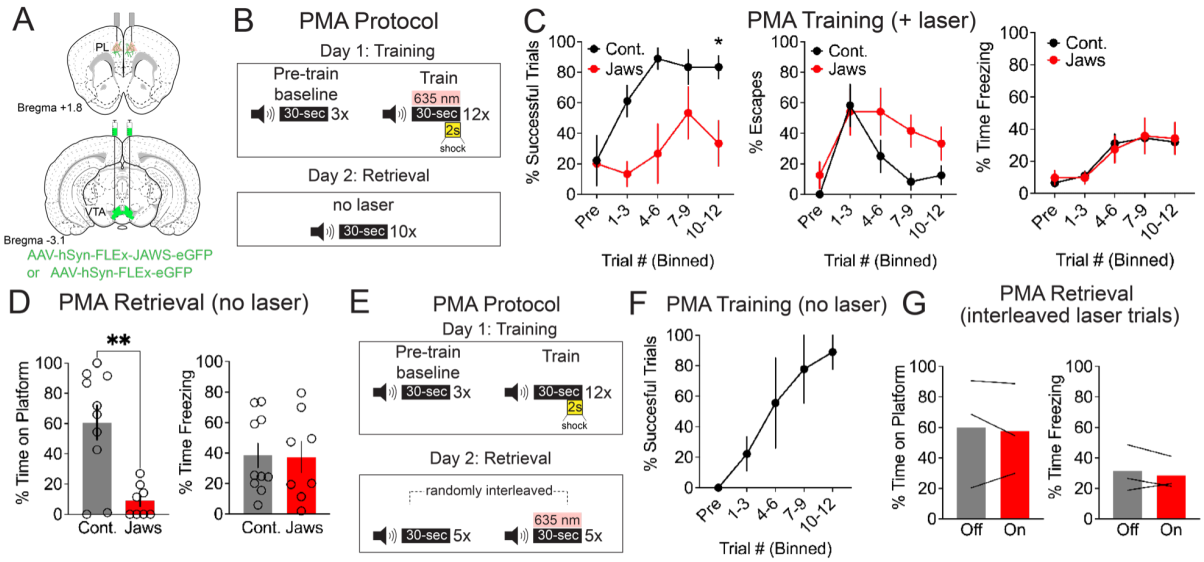

Figure S2. Optogenetic inhibition of VTA-mPFC DA terminals during PMA without motivational conflict.

A. Schematic of viral and fiber optic targeting locations.

B. Protocol for optogenetic inhibition during PMA training. On training day, 635nm laser light was presented coincidently with a 30 second 4kHz tone that co-terminated with a 2-second footshock. On retrieval day, mice were presented with 10 tones without shocks or laser.

C. Fraction of successful trials across days in control vs. Jaws mice ($F_{time}(4.323, 49.71) = 16.66$, $P<0.0001$; $F_{opsin}(1, 13) = 5.092$, $p=0.04$; $F_{interaction}(8, 92) = 2.197$, $p=0.03$; Mixed effects model, N=7 Jaws, N=8 control). Fraction of escape trials across days in control vs. Jaws mice (F_{time} (3.975, 44.71) = 2.33, $p=0.07$; F_{opsin} (1, 12) = 1.68, $p=0.22$; $F_{interaction}$ (8, 90) = 3.09; $p=0.004$. Mixed effects model, N=7 Jaws, N=8 control mice). Fraction time freezing during tone across days in control vs. Jaws mice (F_{time} (4.39, 46.6) = 8.39, $P<0.0001$; $F_{opsin}(1, 11) = 0.60$ $p=0.46$; $F_{interaction}$ (8, 85) = 0.88; $p=0.54$. Mixed effects model, N=7 Jaws, N=7 control mice).

D. Fraction time on platform and fraction of time freezing during tones on retrieval day (platform: $p=0.002$, freezing: $p=0.6$, two-tailed t-test, n=10 control, N=8 Jaws mice).

E. Protocol for optogenetic inhibition during PMA retrieval. Mice are trained in PMA without laser inhibition. The next day, mice are presented with 10 randomly interleaved tones, half of which are paired with constant 635 nm light.

F. Successful trials during PMA training.

G. Percent time on platform and percent time freezing during the tone on interleaved light on and light off trials. *p<0.05, **p<0.01. Plots show mean +/- SEM.

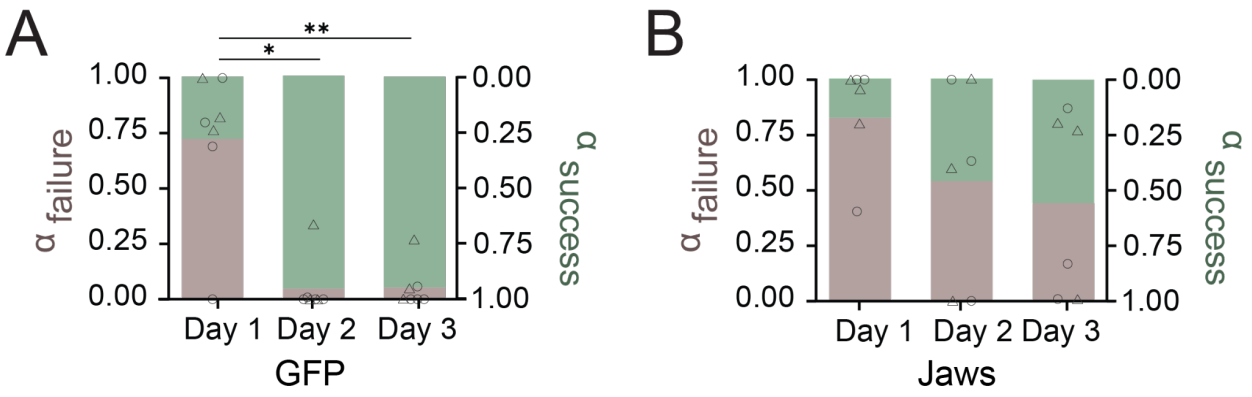

Figure S3. Inhibition of mPFC DA release influences learning rates based on failures and successes.

A. Learning rates per day as calculated by a Rescorla-Wagner model (Figure 3) factoring in trial types (success or failure) for GFP-expressing animals. Model-derived learning rates for GFP animals show a transition from failure-dominant learning to success-dominant learning. Mixed-effects model $F(1.3, 7.4)=20.8$, $p=0.001$. Points represent failure learning rate. *P<0.05, ** P<0.01.

B. Same as A for Jaws-expressing animals. Model-derived learning rates for Jaws animals do not show a change in learning strategy across time. Mixed-effects model $F(1.3, 6.7)=3.1$, $p=0.1$. Points represent failure learning rate.

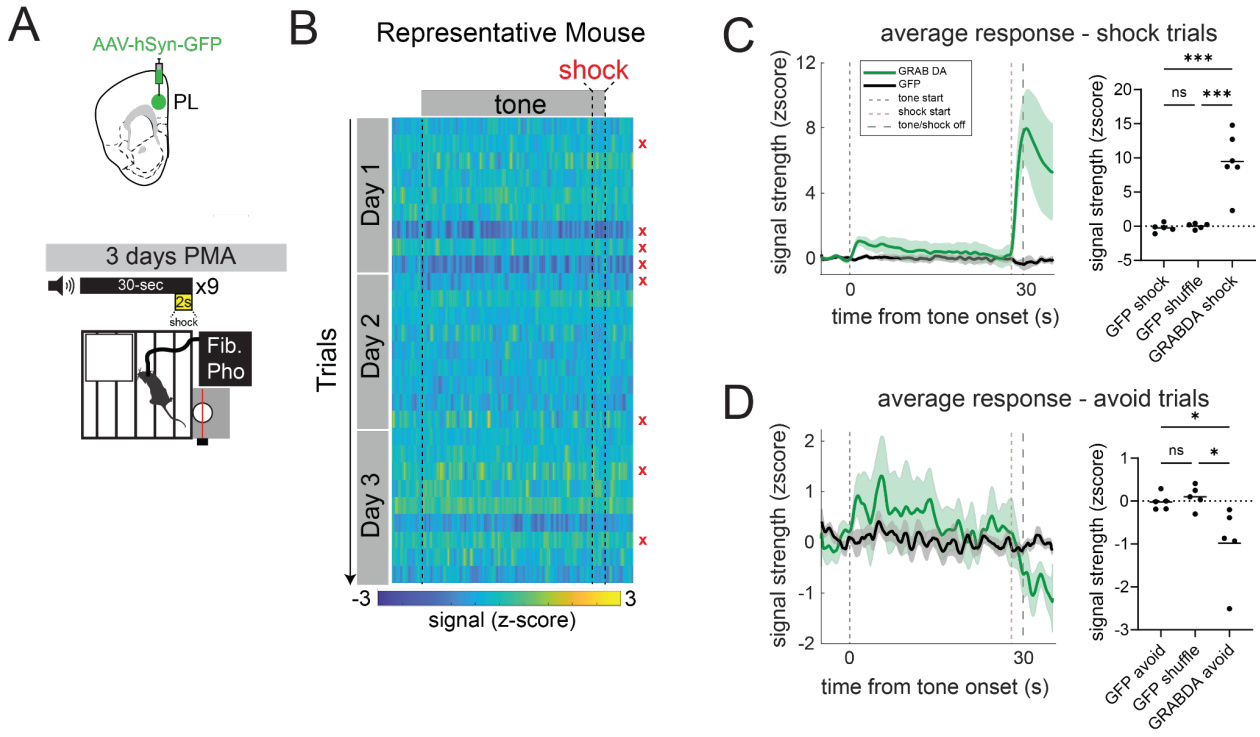

Figure S4. Dopamine responses are not caused by movement artifacts.
A. Surgical strategy to record fluorescent control (GFP) signal in PL (top); schematic of PMA (bottom).
B. Representative heatmap of GFP signal recorded during PMA.
C. GRAB DA animals had increased signal during shock compared to GFP recordings. Averaged signal during shock trials for GFP animals (black) and GRAB DA animals (green) (left). Quantification of shock response in GFP animals, shuffled GFP signal, and GRAB DA animals (right). ANOVA F=22.6, p<0.0001. GFP vs GRABDA p=0.0002, GFP shuffle vs GRABDA p=0.0002, GFP vs GFP shuffle p=0.9. *** p<0.001.
D. GRAB DA animals had decreased signal during shock compared to GFP recordings. Averaged signal during avoid trials for GFP animals (black) and GRAB DA animals (green) (left). Quantification of avoid response in GFP animals, shuffled GFP signal, and GRAB DA animals (right). ANOVA F=6.1, p=0.01, GFP vs GRABDA p=0.02, GFP shuffle vs GRABDA p=0.04, GFP vs GFP shuffle p=0.9. * p<0.05.

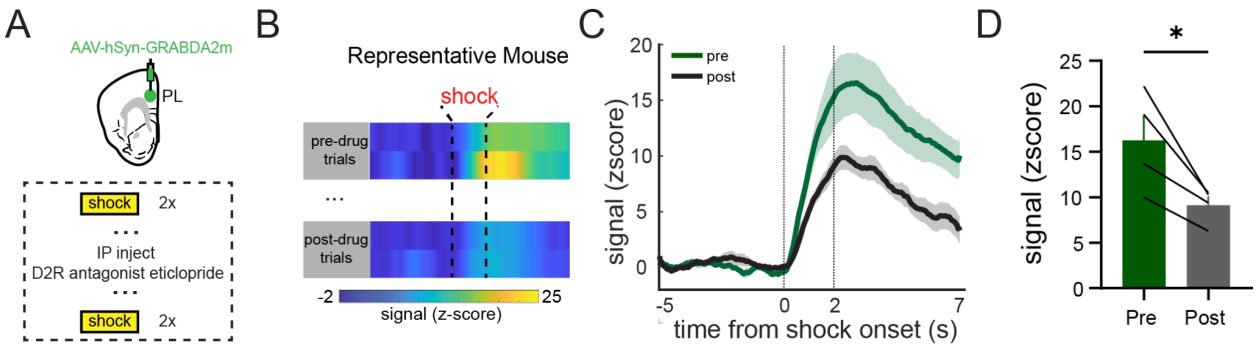

Figure S5. GRABDA response is dependent on D2 receptor function.
A. Experimental schematic: GRABDA signal recorded in PL during shocks prior to then following systemic administration of eticlopride, a D2 receptor antagonist.
B. Representative heatmap of GRABDA signal peri-shock prior to and following eticlopride.
C. Average GRABDA signal peri-shock prior to and following eticlopride.
D. GRABDA shock signal decreases following eticlopride. Paired t-test p=0.03.

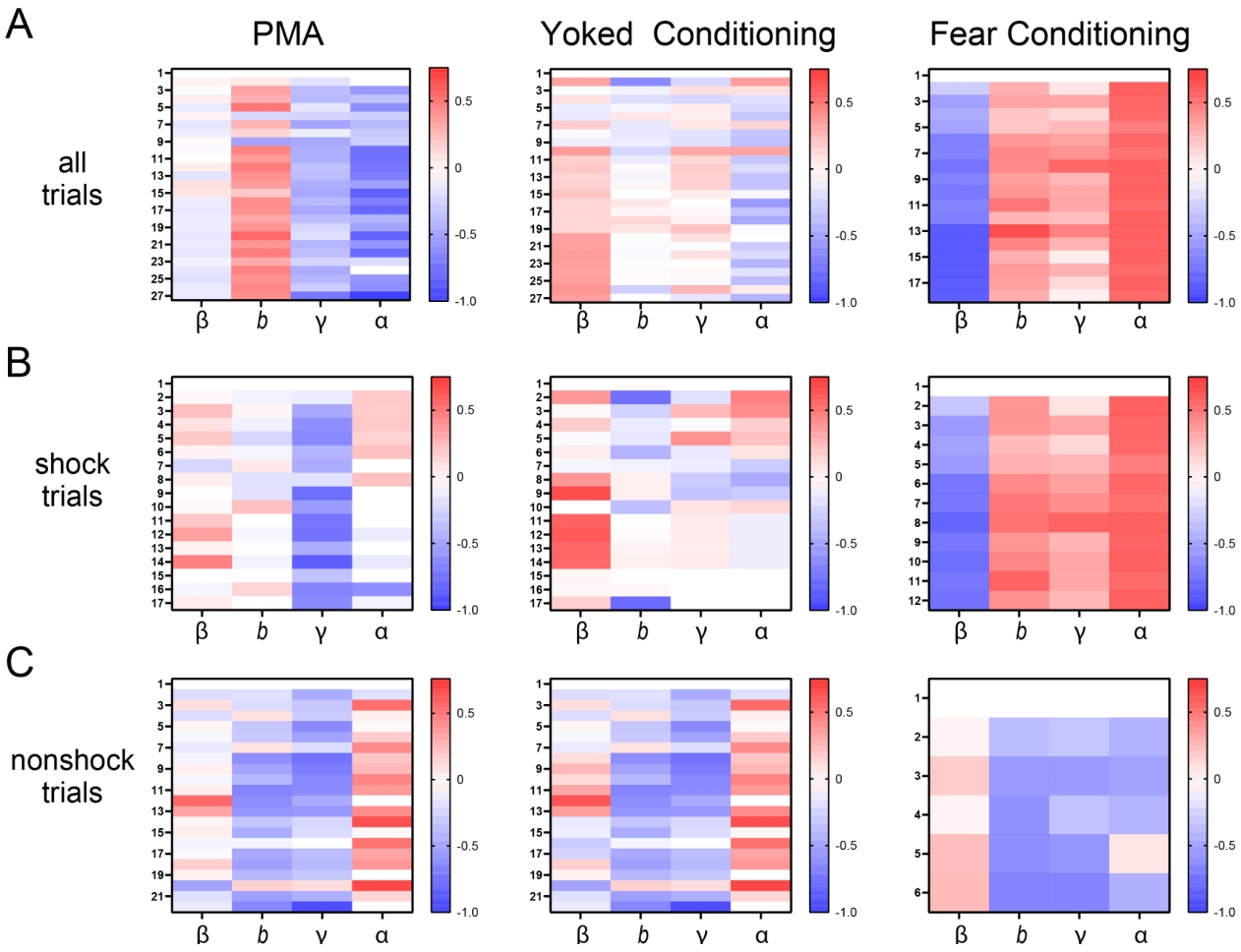

Figure S6. Temporal Difference model parameters across trials.
A. Average parameters displayed across all trials for PMA (left), yoked conditioning (middle), and fear conditioning (right). Values shown as normalized differences from the first trial.
B. Shock outcome only trials. Values presented as normalized differences from the first shock trial.
C. Nonshock outcome only trials. Values presented as normalized differences from the first nonshock trial.
Number of shock and avoid trials in PMA and yoked conditioning differed for each animal but total 27 trials per animal.